Tel-Aviv University

Raymond & Beverly Sackler Faculty of Exact Sciences

Jamming *vs.* Caging in a Three-Dimensional Glassy Model

This thesis was submitted as partial requirement for receiving the degree

Master of Science

School of Chemistry

Department of Chemical Physics

Submitted by

Nimrod Segall

This work was carried under the supervision of

Dr. Yair Shokef and Prof. Haim Diamant

December 2016

Abstract

Glasses are common in everyday life, from a car's windshield to a smart phone's touch screen, the exterior of a light bulb or a drinking cup in the kitchen. While glasses can be produced on an industrial scale with many finely tuned desired properties, glasses, and more so the glass transition – the process by which a material becomes a glass - are very poorly understood from a theoretical point of view and there is not yet a good theory to fully describe glassy behavior. For that reason many different theoretical tools and approaches were developed.

One set of such tools are kinetically-constrained models, which are coarse grained non-interacting lattice models in which the movement of particles is restricted by a set of rules that depend on the state of neighboring sites. In chemistry and physics these models are mainly used to study jamming – a phenomenon where particles in a system become so restricted by their neighbors that they become immobile. Most of these models do not jam at the thermodynamic limit, except when the entire lattice is occupied by particles. There are models, however, which do jam at non-trivial densities, such as the knights model and the spiral model. This thesis focuses on the latter, which are referred to as "jamming percolation models".

In the two dimensional spiral model at the critical jamming density some particles become permanently frozen. The other, unfrozen, particles then become confined in cages formed of frozen particles and their self-diffusion coefficient vanishes. In a recent paper describing a three dimensional model similar to the spiral model, the authors showed that at some critical density jamming occurs, but unlike the two dimensional case, in this three-dimensional model unfrozen particles still diffuse freely in the system. This difference is due to the fact that jamming in these models occurs in the shape of one dimensional objects that in two dimensions act as walls that confine particles to their local environment, while in three dimensions these one dimensional objects do not act as walls as particles can travel around them using the third dimension. The authors predicted the existence of a second critical density at a higher density in which particles will become caged.

In this work we use a fast deterministic numerical algorithm to uncover the underlying structure of the system by identifying the so called unfrozen sites

of the system – the sites of the system which act as free volume for particle movement - which allows us to avoid numerically studying the extremely slow dynamics of the system. We use this structural property of the system to determine whether the system is caging particles to local areas or allowing long range diffusion. We find the caging density and characterize the phase transition at which particles become caged. While the first transition – the jamming transition – is a directed percolation transition, we find that the caging transition's critical exponents are the same as in random percolation, implying the caging transition and the random percolation transition are of the same universality class.

Contents

List of Figures

List of Tables

Nomenclature

β	Critical exponent, $\beta = \frac{\tau-2}{\sigma}$.
Δt	Arbitrary time interval.
Δ	The width of the phase transition.
η	Shear viscosity.
γ	Critical exponent, $\gamma = \frac{3-1}{\sigma d}$
ν	Critical exponent, $\nu = \frac{\tau-1}{\sigma d}$.
ϕ	The size beyond which a cluster is considered infinite.
Π	The probability an infinite cluster exists in the system.
ρ	Initial particle density.
ρ_C	Critical caging density.
ρ_J	Critical jamming density.
τ	Fisher exponent
τ_0	Liquid structural relaxation time.
τ_α	Supercooled liquid structural relaxation time.
ξ_1	Mass of the largest cluster in the system.

A	Prefactor of how the largest cluster in the system scales with system size.
a_d	Typical distance between molecules.
D	Vogel-Fulcher-Tamman law fragility fitting parameter.
d	Dimension of the problem.
d_f	Fractal dimension of the inifnite cluster.
E_B	Energy barrier.
$F_s(q,t)$	Self intermediate scattering function.
G_∞	Shear modulus.
k_B	Boltzmann constant.
L	Linear dimension of the system.
M	Mass (volume) of the infinite cluster in terms of number of sites.
m	Mass (volume) of a cluster in terms of number of sites.
m_BS	Bootstrap percolation; number of nearest neighboring sites that must be occupied for a site to remain occupied.
m_m	Molecular mass.
N	Number of particles in the system.
n_s	Normalized cluster number.
P	Strength of the inifnite cluster, probability a site belongs to the infinite cluster.
p	Occupied sites density / Bond density.

p_{av}	The critical density of the system, shifted due to finite size effects.
p_{RP}	Critical random percolation density.
Q	Probabilty a site on the Bethe lattice is not connected to inifnity through a given branch.
q	Wave vector.
r	Particle position.
r_c	Cooling rate.
r_{rad}	Radius.
S	Mean cluster size.
s	Size of a cluster in terms of number of sites.
s_T	Mean cluster size that belongs to a branch of a site on the Bethe lattice.
s_{max}	The mass of the largest finite cluster.
T	Temperature.
t	Time.
T_0	Temperature in which τ_α diverges according to the Vogel-Fulcher-Tamman law.
t_0	Initial time.
T_g	Glass transition temperature.
T_m	Melting temperature.
z	Coordination number.

Chapter 1

Theoretical Background

In this chapter we will first discuss glasses, their importance, and the glass transition problem. We will see to some extent why glasses are difficult to accurately model and will give some intuition as to why there are so many different approaches to tackling this subject. We will then proceed to discuss percolation theory - which will serve as an important tool in Chapter 3, where the methods we used to analyze our results were heavily influenced by those used in percolation problems. Finally, we present kinetically constrained models in general and the particular model studied in this thesis.

1.1 Glasses

1.1.1 Introduction

Glasses are common in everyday life, and while they are easily designed on an industrial scale with desired optical or mechanical attributes, a deep microscopic understanding of glasses is still absent. One of the intriguing points regarding glasses is that they appear rigid on a macroscopic scale like solids, and yet are disordered at the molecular level like liquids [2, 3]. A fluid is considered a glass if it is supercooled below its glass transition temperature T_g. The quenching must

be done in such a way that the standard first order liquid-solid phase transition that we normally see at the melting temperature of the material (T_m) does not occur, usually by means of applying a cooling rate to the system which is faster than the nucleation rate of the crystal phase [3, 31], see Fig. 1.1.

Unlike standard thermodynamic phase transitions, the glass transition is not an equilibrium transition and the glass transition temperature T_g is not an exact value derived from the statistical thermodynamics of the system but an operational temperature below which matter behaves like a solid - at least on an experimental time scale. Pragmatically this temperature is usually defined as the point at which the shear viscosity η reaches $10^{13}\, Poise$ [3]. However as we will see in the next section the relaxation times of the system increase exponentially with temperature as we approach T_g. Hence glass transition temperature is sometimes defined in direct relation to the experimental time scale by simply stating that T_g is a point at which the longest relaxation time of the system exceeds $\frac{1}{r_c}$, r_c being the cooling rate of the experiment or simulation. Below T_g fluids slowly evolve in time. Whether they eventually reach equilibrium or not still remains an open question. The system's physical properties slowly evolve in a far from equilibrium non-ergodic state and the system is said to be **aging**. For further details on these topics please see [3].

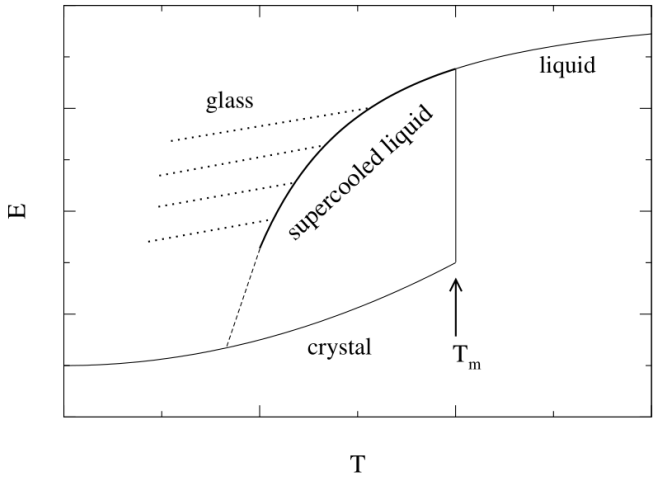

Figure 1.1: A schematic plot of the system's energy E as a function of temperature T. The continuation of the liquid line at $T < T_m$ shows the supercooled regime which is extrapolated with a dashed line to a point where it reaches the crystalline state, in which, theoretically, the system may undergo a phase transition from a supercooled liquid to a crystal. The four dotted lines correspond to four different cooling rates. Adapted from [25].

1.1.2 The Glass Transition - Critical Behavior

T_g is an arbitrary point and thus we may be lead to believe it has no special physical importance. However, we can still find interesting effects in the glass transition, namely exponential scaling of the relaxation times with temperature. For example, if we consider τ_α, the relaxation time of fluctuations in density, at T_m the melting temperature it is of the order of $\sqrt{\frac{m_m a_d^2}{k_B T}}$ [3] (can be derived from a dimensional analysis approach) which is typically about a few picoseconds (m_m being the molecular mass, a_d the typical distance between molecules, T the temperature and k_B is the Boltzmann constant). However, at T_g this relaxation time becomes of the order of 100 seconds. This remarkable 14 order of magnitude factor between the two time scales, which typically corresponds to a change of only about a third in temperature (as a rule of thumb $T_g \sim \frac{2}{3} T_m$ [9]), a relatively small difference as the typical energy scale is $k_B T_m$. When τ_α is increased the

shear viscosity also increases. This should not come as a surprise: if we assume a Maxwell material, that is that the system can be described by a purely viscous damper connected to a Hookean spring in a series, we can relate viscosity to the relaxation time through $\eta = G_\infty \tau_\alpha$ where G_∞ is the elastic modulus and depends weakly on temperature. We get an extremely viscous material which macroscopically appears rigid on an experimental time scale.

In Fig. 1.2 the (logarithm of) relaxation time is plotted as a function of (the inverse) temperature. These plots are referred to as Angell plots[2], and are helpful in the classification of supercooled liquids. A straight line would imply an Arrhenius behavior, that is where we have an exponential barrier of some fixed energy which acts as the only energy scale in the system:

$$\tau_\alpha = \tau_0 exp\left[\frac{E_B}{k_B T}\right], \tag{1.1.1}$$

(where E_B is the activation energy and τ_0 is the liquid's relaxation time) and a material behaving this way would be considered a **strong** glass. As seen in the Angell plot figure, many materials do not behave in an Arrhenius fashion and actually exhibit a super-Arrhenius behavior. These would be considered **fragile** glasses. The terms strong and fragile glasses do not refer to the actual rigidity of the material, but in fact to the evolution of short range order near T_g, this is explained in more detail in Section 1.1.3.

There are many ways in which one can try fitting these curves, but one common attempt is given by the Vogel-Fulcher-Tamman law:

$$\tau_\alpha \sim exp\left[\frac{DT}{(T - T_0)}\right]. \tag{1.1.2}$$

D is a dimensionless fitting parameter, and the smaller D is the more fragile the glass is. This suggest that at some temperature T_0 the relaxation time actually diverges and the system undergoes some phase transition. This singularity however should not be discarded so quickly as just an artifact of the fitting function,

as mode coupling theory [14] - a commonly used theory for glass formers - also predicts a divergence. It should also be emphasized that while the Vogel-Fulcher-Tamman law is a common one, there exists other good fits that do not predict divergence of the relaxation time, and that due to the long time scales of these systems getting a good measurement near this predicted T_0 is not possible.

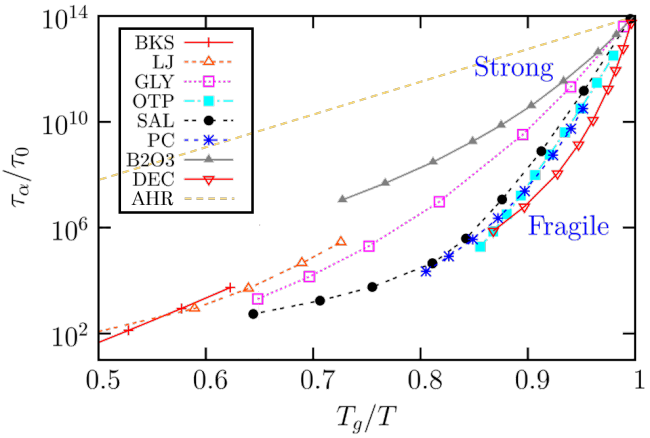

Figure 1.2: Angell plots of the relaxation time of several materials approaching the glass transition temperature T_g. τ_0 is the relaxation time of the liquid phase. By definition the glass transition occurs when $\frac{\tau_\alpha}{\tau_0} = 10^{14}$ and so at that point $\frac{T_g}{T} = 1$. BKS - numerical model of silica, LJ - numerical model of a binary Lennard-Jones mixture, GLY - glycerol, OTP - ortho-ter- phenyl, SAL - salol, PC - propylene carbonate, DEC - decaline, AHR - Arrhenius behavior with with $\exp\left(\frac{E_B}{k_B T_g}\right) = 10^{14}$. Adapted from [3].

1.1.3 Dynamical Heterogeneities - Cooperative Motion

The non-Arrhenius behavior of the relaxation time in glass-forming liquids may imply the system has multiple relaxation times [31]. This notion is further supported by looking at the self-intermediate scattering function:

$$F_s(q,t) = \left\langle \frac{1}{N} \sum_{j=1}^{N} \exp\left[iq\left(r_j(t-t_0) - r_j(t_0)\right)\right] \right\rangle. \tag{1.1.3}$$

Here the $\langle\rangle$ brackets indicate ensemble average, N is the total number of particles in the system, i is the imaginary unit, r_j is the position of the j'th particle, t is the time, t_0 is the initial time and q is a wave vector (resulting from a Fourier transform). The self-intermediate scattering function takes into account the position correlation of some specific particle over time $t - t_0$ and averages over all particles in the system and over the statistical ensemble of all possible realizations of system. For some specific $q = q'$, in any time interval Δt for which $F_s(q, \Delta t) > 0$ the system retains memory of its previous states and thus is non-ergodic. Therefore the system reaches full relaxation only for time intervals $\Delta t'$ long enough so that $F_s(q, \Delta t) = 0$.

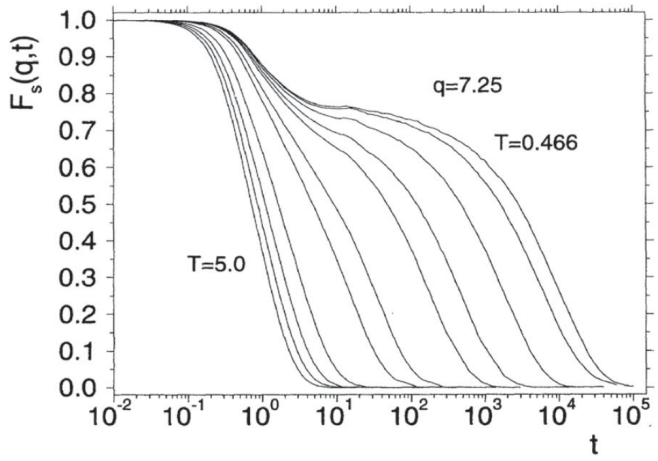

Figure 1.3: The self-intermediate scattering function $F_s(q, t)$ for a simulated glass-former composed of two types of particles A and B interacting via a Lennard-Jones potential. F_s is calculated only for positions of particles of type A. Here $q = 7.25$ corresponds the largest peak in the static structure factor. Difference curves correspond to different temperatures. Adapted from [1].

As seen in Fig. 1.3, at high temperatures $F_s(q, t)$ decays exponentially, as it would in a normal liquid. This implies the existence of a single microscopic time scale. However, as temperature is lowered a plateau is formed, which spans over increasingly longer time scales as temperature is decreased. This plateau can span over several decades in which the system retains memory, and only after which

the system relaxes completely and ergodicity is obtained. The second part of the decay has the shape of a stretched exponent, which implies a broad spectrum of relaxation processes rather then a single relaxation time. One explanation to this phenomenon may be that the relaxation times in glass formers is intrinsically non-exponential in time. Another explanation to this stretched exponent behavior may reside in the non-homogeneous microscopic structure of glass formers. If different regions have different relaxation times then if we average over all particles and over the ensemble we may find this sort of non-exponential behavior [3]. While both explanations are supported by evidence from simulations and experiments, the latter can be visually illustrated in Fig. 1.4. Here we can see the displacement of different particles over some period of time. Different regions are observed: active regions, where particles are mobile, and inactive regions where particles stay local. More details on these subjects are covered in [3].

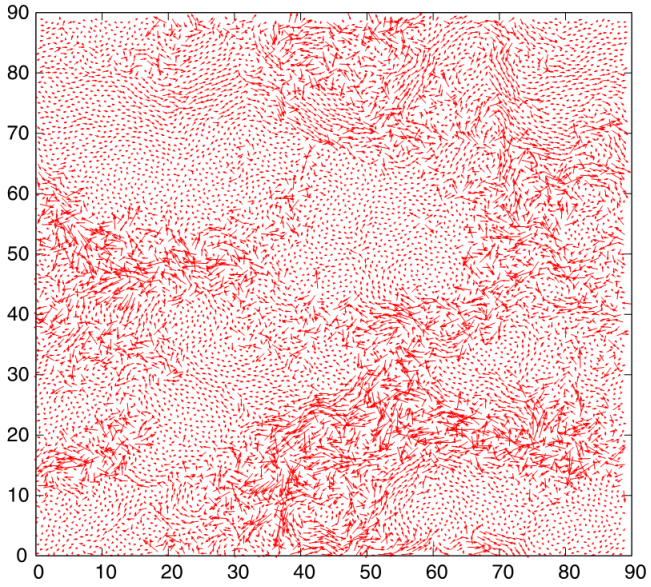

Figure 1.4: Results of a numerical two dimensional Lennard-Jones binary mixture simulation. Red arrows show the displacement of each particle in a set time interval. Different regions can be seen side by side. Active regions where particles are mobile, and inactive regions where particles barely move at all. Adapted from [3].

As seen in this brief introduction, the glass transition is a complicated matter and glassy dynamics are tricky to properly model. Due to that many different approaches are used. One tool commonly applied to these problems is related to percolation theory which is reviewed in the next section.

1.2 Percolation Theory

1.2.1 Random Percolation

In this section we will give a brief introduction to percolation theory, and show how basic percolation problems are solved. More importantly we will review the concepts of the infinite cluster and the mean cluster size, and how these are used to analyze the system which will become crucial in Chapter 3 where we will discuss data we acquired from simulation and use these very tools to present our results.

Percolation theory is used in many fields. Notable examples of which include the study of epidemic outbreak within a population[22], the dynamics of forest fire spreading[6] and the gelation process of polymers[7]. One may use these sort of models to describe water percolating through a porous rock; here sites represent vacancies in the rock and if a cluster of such sites would connect the top of the rock to the bottom of it then water could flow via a path in that cluster.

There are two main types of percolation problems: site percolation, and bond percolation, See Fig. 1.5. Both are usually defined on a lattice and are studied at the limit where the linear dimension of the system L is very large. In a site percolation problem we randomly occupy sites on the lattice until we reach an occupied site density p. Nearest neighbors are then considered to be connected and connected clusters of sites are formed. In a bond percolation problem every lattice site is considered occupied, and initially all sites are not connected. We then randomly add bonds between nearest neighbors until we

reach a bond density p. Occupied sites that have a bond between them are then considered connected and clusters of connected sites are formed. In both cases we then want to learn if there exists a cluster of occupied sites on the lattice so that it reaches from one end of the system to the other, which would make it infinite in the thermodynamic limit, when we take $L \to \infty$. We refer to this as the **infinite cluster**. To further our understanding of the system, we would commonly like to analyze the distribution of clusters formed in the system.

The formation of such an infinite cluster occurs at some specific critical density p_{RP} and this transition is referred to as the **random percolation transition** - since sites are being occupied at random. Interestingly this infinite cluster tends to have a peculiar structure at p_{RP} [33]. Consider a two dimensional system and ask how the mass (or volume) of the infinite cluster, M, changes with the size of the system. We might expect the answer to be length raised to the power of the Euclidean dimension, that is $M \sim L^2$. However, simulations show [33] that the scaling relation is actually $M \sim L^{d_F}$ where $d_f = 1.9$. d_f is called the **fractal dimension** of the infinite cluster, since in percolation problems it is often the case where at the critical point the infinite cluster's mass scales as length to the power of a number which is only a fraction of the Euclidean dimension.

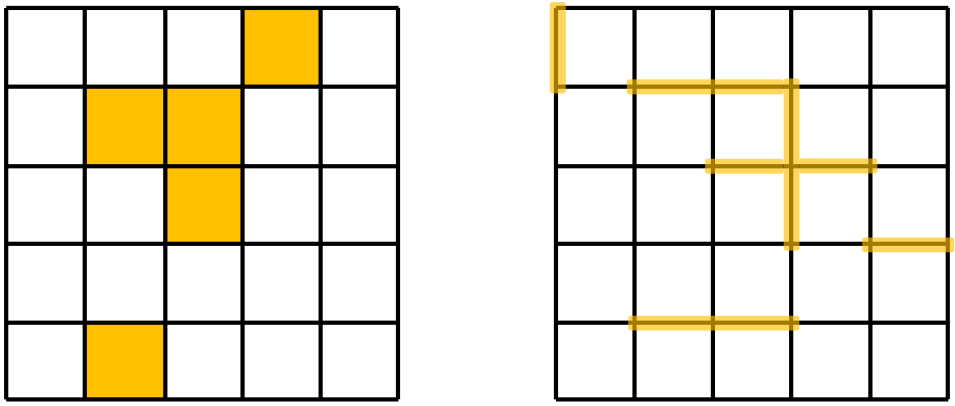

Figure 1.5: Site percolation vs bond percolation. Adapted from **mathworld.wolfram.com**.

Random percolation is not the only type of percolation. Another commonly used type of percolation is **bootstrap percolation [5]**, where after the system is set and sites have been randomly occupied, sites without m_{BS} nearest neighbor occupied sites are rendered vacant and only then the process of cluster analysis begins. Another type of percolation is called **directed percolation**, and undergoes a directed percolation transition at a critical density denoted by p_{DP}. In a directed percolation problem for a set of sites to be considered a cluster it is not enough that they are connected, but they must also follow some direction or directed path, See Fig. 1.6. For example if we wanted to describe water percolating through small cracks in a porous rock, we may not want water to be able to flow up against gravity [12]. In such a case having a cluster reaching from the top of the system to the bottom of it is not enough, as if that cluster curves upwards water may get stuck down the curve. In a random percolation problem all sites connected are members of the same cluster, regardless of which site we choose as an origin from which we check connectivity. In a directed percolation problem the choice of origin may exclude sites from the cluster, and as such is

more restrictive than random percolation and due to that $p_{RP} < p_{DP}$.

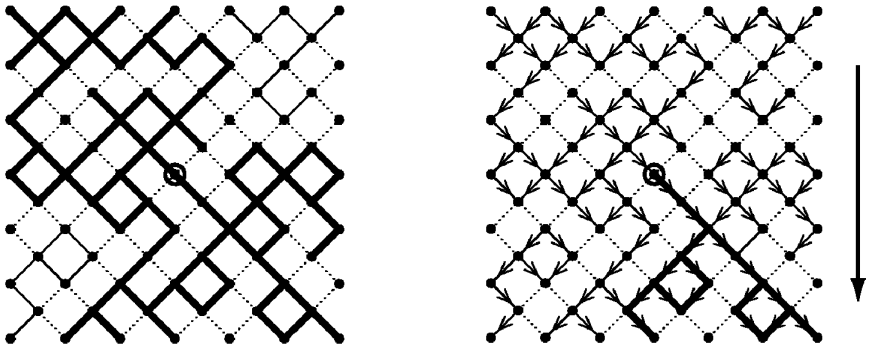

Figure 1.6: Comparison between random (isotropic) bond percolation and directed bond percolation. The circled site in the center is the point of origin. Thin solid black lines are bonds connecting sites on the lattice. The thick black lines are all bonds that connect sites belonging to the cluster of the origin site. The direction for the directed percolation case is down, indicated by arrows over bonds. For random percolation all sites connected together are a part of the same cluster. For the directed percolation case only sites which can be reached by means of traveling over existing bonds pointing down are allowed. One could imagine that water injected to the point of origin would flow downwards reaching only the sites indicated by the directed percolation image. Taken from [12].

In the next subsections we will show basic examples of random site percolation problems. By solving them. we will introduce important concepts regarding the random percolation transition, which we will later study in the context of caging of particles in our glassy model.

1.2.2 One Dimensional Random Site Percolation

Assume a chain of length $L \gg 1$ (L is expressed in terms of the number of sites), in which every site is occupied with probability p and unoccupied with probability $1-p$ [33]. The question of in which occupied site density p there exists an infinite cluster that reaches from one end to the other becomes trivial in the one dimensional case, since all sites must be occupied in order for a cluster like that to exists, and so $p_{RP} = 1$. The one dimensional case is therefore rather simple, and unlike many other percolation problems the regime of $p > p_{RP}$ does not exist here. We can, however, still observe the distribution of cluster sizes in the system. A cluster of size s is a sequence of s consecutive occupied sites. However, if we include the vacancies in the edges it comprises, an unoccupied site, then s occupied sites, and at last another unoccupied site. The probability a certain site is, for example, the left end of a cluster of size s is then $(1-p)\,p^s\,(1-p) = p^s\,(1-p)^2$. This of course disregards the edges of the system, however for $L \gg 1$ edge effects are negligible. If so, the system contains $L \cdot p^s\,(1-p)^2$ clusters of size s, or if we would like to consider the number of clusters of size s per lattice site we divide by L and get:

$$n_s = p^s\,(1-p)^2\,, \tag{1.2.1}$$

n_s is called the **cluster number**, and is a useful measure in percolation problems.

We may also want to ask, if we select a site which is part of a finite cluster at random, how big on average would that cluster be. There is a probability $n_s s$ that an arbitrary site (occupied or not) belongs to a finite cluster of size s, and there is a probability $\sum_s n_s s$ that it belongs to any finite cluster, and so

$$w_s = \frac{n_s s}{\sum_s n_s s}, \tag{1.2.2}$$

is the probability the cluster to which an arbitrary occupied site belongs to is of

size s. If so, the **mean finite cluster size** is:

$$S = \sum_s w_s s = \sum_s \frac{n_s s^2}{\sum_s n_s s}. \tag{1.2.3}$$

This is a general expression. Plugging Eq. (1.2.1) into Eq. (1.2.3) we get the mean cluster size for the one dimensional case:

$$S = \sum_s \frac{p^s \cdot s^2}{\sum_s p^s \cdot s}. \tag{1.2.4}$$

In the limit where we approach the critical density $p \to p_{RP} = 1$ and the finite clusters become increasingly big we get

$$S = \frac{1+p}{1-p}. \tag{1.2.5}$$

We should note that in general we sum only over finite clusters, excluding the infinite cluster. Also, this mean cluster size is the average cluster size **per site** and **not per cluster**. The one dimensional random percolation problem might not be very exciting, as we cannot explore the regime of $p > p_{RP}$ since as we have seen $p_{RP} = 1$. In the next subsection we will solve the random percolation problem on a Bethe lattice in an attempt to give some more intuition regarding the nature of percolation problems.

1.2.3 Random Site Percolation on a Bethe Lattice

A Bethe lattice, also known as a Cayley tree, is a graph constructed such that each node in the graph has the same number of neighbors, z, and that there are no loops. More so, we investigate it at the thermodynamic limit where the number of sites is very large. The Bethe lattice gives us some insight regarding high dimensional systems [33]. One reason is that in high dimensions the probability of finding loops is small. For example in a hypercubic lattice the number of ways to embed a four site chain in d dimensions is proportional to $(2d-1)^3$ while

the number of ways to have four sites that generate a loop is proportional to $d\,(d-1)$, so $\lim_{d\to\infty} \frac{d(d-1)}{(2d-1)^3} = 0$, and so this justifies the fact the Beth lattice does not have any loops. Another reason is that in d dimensions volume normally scales as r_{rad}^d and surface area scales as r_{rad}^{d-1} (r_{rad} being a relevant length scale. For example for a hypersphere the radius). In high enough dimensions the surface area and volume are about the same, as $d \sim d-1$ for large d [33]. Similarly on the Beth lattice if we consider a sphere, that is all the sites within distance r_{rad} from some origin site, both the surface area and the volume scale as $(z-1)^{r_{rad}}$. While these are all hand-waving sort of arguments, they do provide some intuition as to why the Bethe lattice may share similarities with systems of high dimensions.

We define all sites connected from the same neighbor to that central site as a branch. Similarly, all sites connected to a neighbor of the central site via the same next to nearest neighbor as a subbranch. See Fig. 1.7.

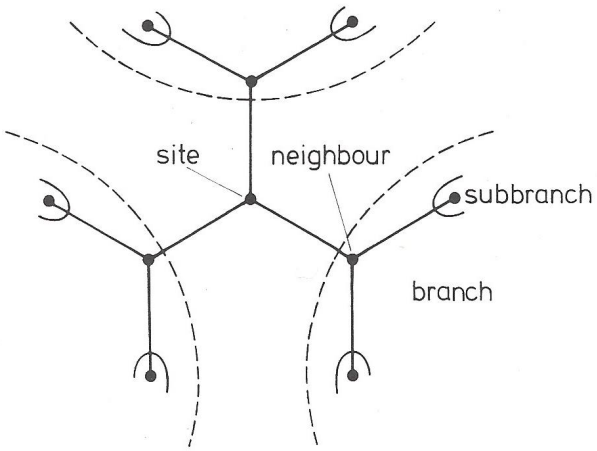

Figure 1.7: The Beth lattice for $z = 3$. Around the central site are the branches, and around those are the subbranches. Adapted from [33].

To find the percolation threshold p_{RP} we start at some site and check to see if we can expand outwards in an infinite path through any of the branches. There are $z-1$ new sites emanating from each neighbor, which is occupied with probability p and thus on average we have $p\,(z-1)$ new occupied sites that are

added to the cluster per neighbor. If this number is smaller than unity, that is $p(z-1) < 1$ then on average we gain less than one new occupied site to the cluster as we progress along the branches. For an infinite cluster to exist, we must have $p(z-1) \geq 1$.This yields the percolation threshold:

$$p_{RP} = \frac{1}{z-1}. \tag{1.2.6}$$

Let us now calculate the **strength of the infinite cluster** P - that is the **probability that a site belongs to the infinite cluster**. For simplicity we will assume $z = 3$ but the problem can be solved in a similar way for any value of z. We define Q as the probability that an arbitrary site is not connected to infinity through one specific branch. The probability that the two subbranches in a given branch are not connected to infinity is Q^2. This is due to the fact that any two sites in the system are equivalent, and so the probability a branch does not connect to infinity is the same as the probability a subbranch does not connect to infinity, and that these two subbranches are independent of each other. Thus pQ^2 is the probability a neighbor is occupied but does not connect to infinity through its subbranches. This neighbor is empty with probability $1-p$, and if it is empty then it does not matter if its subbranches connect to infinity. And thus we can write:

$$Q = 1 - p + pQ^2. \tag{1.2.7}$$

Solving for Q we get two solutions: $Q_1 = 1$ and $Q_2 = \frac{1-p}{p}$. The probability $p - P$, that the origin is occupied but is not connected to infinity through either branch is pQ^3, and thus

$$P(Q) = p\left(1 - Q^3\right). \tag{1.2.8}$$

$P(Q = Q_1) = 0$, which implies this solution is valid for $p < p_{RP}$, where the infinite cluster does not exist. On the other hand for Q_2 we find

$$P(Q = Q_2) = p\left[1 - \left(\frac{1-p}{p}\right)^3\right]. \tag{1.2.9}$$

In a similar way we can calculate the mean finite cluster size S. Let s_T be the mean size of a cluster that belongs to one branch. The subbranches have the same mean cluster size, since - as before - all sites are equivalent. If the neighbor is occupied it contributes its own mass plus the mass of its two subbranches. If it is unoccupied then it does not contribute at all. Therefore we can write

$$s_T = p \cdot (1 + 2s_T) + (1 - p) \cdot 0 = p\,(1 + 2s_T)\,, \tag{1.2.10}$$

and so we find $s_T = \frac{p}{(1-2p)}$. The total mass of the cluster connected to the central site is zero if the central site is empty, and is $1 + 3s_T$ if it is occupied (1 for the site itself and a factor of s_T for every branch) and so we get:

$$S = 1 + 3s_T = \frac{1+p}{1-2p}. \tag{1.2.11}$$

On the Bethe lattice, unlike the one-dimensional case, we have access to the regime of $p > p_{RP}$ (for any $z > 2$), meaning we can investigate the behavior of $P\,(p)$ and $S\,(p)$ near the critical point. Just under $p < p_{RP}$ an infinite cluster does not yet exist, and one may expect that S will become very large, as it takes into account this almost infinite cluster. If we take Eq. (1.2.6) and set $z = 3$ we find $p_{RP} = \frac{1}{2}$. We then take the series of Eq. (1.2.11) and expand it in a Taylor series to first order in p at $p = p_{RP}$. This gives $S \approx -\frac{1}{p-p_{RP}}$, or alternatively

$$S \propto (p - p_{RP})^{-\gamma}\,, \tag{1.2.12}$$

with $\gamma = 1$, meaning S diverges at p_{RP}.

On the other hand at $p = p_{RP}$, we have $P = 0$. We can verify this by setting $p = \frac{1}{2}$ at Eq. (1.2.9) and so we may expect it to be small for values just above the critical density. Indeed, if we take the first order term of Eq. (1.2.9) we find $P \approx 6\,(p - p_{RP})$, or

$$P \propto (p - p_{RP})^{\beta}\,, \tag{1.2.13}$$

With $\beta = 1$. These results are to be expected, as the percolation transition is

a (second order) phase transition, and as such we expect the order parameters of the problem to behave according to a power law as a function of distance from the critical point. Here γ and β are critical exponents that help define the universality class of this transition, and while their values are trivial in this simple Bethe lattice model in other models and dimensions calculating their exact value may become more difficult.

In the following section we will discuss kinetically constrained models, which are a class of simplistic dynamical models which are closely related to percolation, and which can contribute to the understanding of the glass transition.

1.3 Kinetically Constrained Models

Kinetically constrained models [25] are a class of simplistic lattice models used in various fields, such as vapor deposition [19], DNA polymerization [20], traffic [8], and disease spreading [16]. In the fields of chemistry and physics kinetically constrained models are most commonly used to describe glassy dynamics and colloidal systems, and for studying jamming [25]. There are two main types of kinetically constrained models: spin facilitated Ising models and constrained lattice gases. Both have stochastic Markovian dynamics and obey detailed balance with respect to some trivial Hamiltonian. As suggested by their names, kinetically constrained models obey certain constraints forbidding some local transitions between configuration. In the case of spin facilitated models the constraint is placed on spin flipping, while in the case of lattice gases the constraint is placed on the movement of particles between neighboring sites. In this section we will present several commonly used kinetically constrained models, and most notably the spiral model, which is the two-dimensional ancestor of the model we studied.

1.3.1 Spin Facilitated Models - Fredrickson-Andersen Model

The Fredrickson-Andersen model [10] is a spin facilitated model defined in d dimensions on a (hyper-)cubic lattice. In total there are $N = L^d$ sites (L being the length of the system and d the dimension), each set with an initial state of $\sigma = 1$ with probability ρ or of $\sigma = 0$ with probability $1 - \rho$. Sites with a state $\sigma = 1$ are referred to as active, which correspond to areas of the system with low density while sites with state $\sigma = 0$ are referred to as inactive, and correspond to areas of the system where the density is high. We assume there are no interactions between sites and so the Hamiltonian of the system is trivial:

$$H = \sum_{i=1}^{N} \sigma_i \tag{1.3.1}$$

Each spin tries to flip with rate $w(1 \to 0)$ for flipping from active to inactive and $w(0 \to 1)$ for flipping from inactive to active, and is successful if some local constraint related to its neighboring sites is fulfilled. In the Fredrickson-Andersen model that local constraint is that a site trying to flip must have at least f nearest neighbors that are active, i.e with $\sigma = 1$. Spins that do not fulfill this constraint are considered **blocked**, and cannot flip until their local environment changes. Since this rule does not depend on the state of the site flipping but merely depends on the state of neighbors, once flipped, a site could flip back in the next time step. Therefore for any given allowed path of spin flips in phase space the system could choose to traverse the reverse path.

The system's Hamiltonian depends only on the number of active sites, and so since each state occurs with probability proportional to its Boltzmann weight $e^{-\frac{H}{k_B T}}$ every state with the same density of active sites occurs at an equal probability. However, these spin flipping dynamics do not conserve the number of active sites and so we want to choose the rates $w(1 \to 0)$ and $w(0 \to 1)$ so that detailed balance is maintained. The difference in energy between a state

where one spin flips is ± 1, and so we can calculate the rate of transition according to Metropolis dynamics [18] using

$$w\left(1 \to 0\right) = 1, \tag{1.3.2}$$

$$w\left(0 \to 1\right) = e^{-\frac{1}{k_B T}}, \tag{1.3.3}$$

or using Glauber dynamics [18, 25]:

$$w_{\pm} = \frac{1}{1 + e^{\frac{1}{k_B T}}}. \tag{1.3.4}$$

1.3.2 Lattice Gas Models - Kob-Andersen Model

The Kob-Andersen model [17] is a lattice gas version of the Fredrickson-Andersen model. Here a lattice site with state $\sigma = 1$ corresponds to a particle, and a site with state $\sigma = 0$ corresponds to a vacancy, and so ρ corresponds to the particle density in the system. Each particle tries to move with rate W_{KA} and is successful if some local constraint related to its neighboring sites is fulfilled. In the Kob-Andersen model, similarly to the Fredrickson-Andersen case, the constraint is that a particle trying to move must have at least f nearest neighbors that are empty, i.e with $\sigma = 0$, and that constraint must be maintained both before and after a particle had moved, so that the time reversible dynamics are retained. Similarly, when a particle does not satisfy the kinetic constraint of the model, that particle is considered **blocked** and cannot move until its local environment changes. Since the same trivial Hamiltonian at Eq. 1.3.1 applies to all kinetically constrained models, here too all states with the same number of particles have the same Boltzmann weight and thus the same probability of occurring. However, unlike the Fredrickson-Andersen model the number of particles remain constant and so to conserve detailed balance any rate of transition W_{KA} will do. In the Kob Andersen model (and generally in kinetically constrained lattice gas models) particle tend to move almost simultaneously. This is due to the fact that in order for a particle to move its local environment must have enough vacancies, and a

particle must jump to one of these vacancies. If density is high enough when a particle moves it creates an opportunity for its neighbor to move, which in turn creates opportunities for their neighbors, and so on [35, 34]. Thus the dynamics are cooperative.

1.3.3 Jamming - Frozen and Unfrozen Particles

Due to the cooperative dynamical nature of kinetically constrained models, as density is increased the mobility of particles is decreased. This happens because in higher densities particles become blocked for longer periods of time and must wait for more neighboring particles to move before a vacancy that can facilitate movement is formed[34]. When density has increased enough, the system reaches a critical density ρ_J beyond which, some particles become permanently blocked. Beyond this critical density at $\rho \geq \rho_J$ the system is said to be **jammed** and the permanently blocked particles are referred to as **frozen particles**. Since dynamics are time reversible in kinetically constrained models, whether a particle is frozen or not is determined when initial conditions are set, and this does not change as the system develops dynamically in time. In spin facilitated models a similar phenomenon can occur, where spins become permanently blocked and thus become frozen. Since a certain number of neighboring sites are required to be vacant or active, respectively, the Kob Andersen and the Fredrickson Andersen models undergo jamming associated with bootstrap percolation [26]. However, in the thermodynamic limit it has been shown that for both models the critical jamming density is trivial: $\rho_J = 1$ [13, 35].

In the next sub-section we will present the spiral model, in which jamming is associated with directed percolation and in which the jamming density is non-trivial even in the thermodynamic limit.

1.3.4 Jamming Percolation Models - The Spiral Model

Jamming percolation models [15] are a relatively new type of kinetically constrained models which better capture the essence of the glass transition [36]. These models undergo a jamming transition at some non-trivial density $\rho_J < 1$ in which some major fraction of the particles in the system become frozen. These systems are characterized by having a restricting set of kinetic rules that can be mapped to a **directed percolation** problem. A notable such model is the **spiral model** [4] which has a rule set under which the model undergoes a **mixed order** phase transition at a critical density $\rho_J \approx 0.705$, which is the critical density of a directed percolation transition in two dimensions.

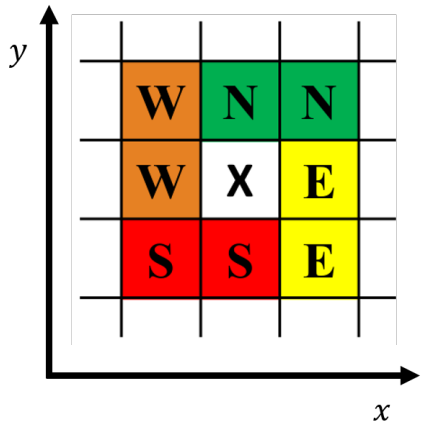

Figure 1.8: The four groups that neighboring sites are divided to: **North**, **South**, **West** and **East**. Site$[X]$ is unblocked if its (**N** or **S**) and (**W** or **E**) groups are completely empty.

In the spiral model we divide the neighbors of each site to four different sets, each containing two sites as seen in Fig. 1.8: **North**, **South**, **West** and **East**. We define new logical variables: $\tilde{N}$, $\tilde{S}$, $\tilde{W}$, $\tilde{E}$, each corresponds to North, South, West an East sets respectively. A variable is true if the corresponding set is occupied on both sites, and false otherwise. We demand that for a site to be considered unblocked the condition $\left(\tilde{N} \vee \tilde{S}\right) \wedge \left(\tilde{W} \vee \tilde{E}\right)$ is true. groups

are completely empty, where are logical variables which are true if . The result of these kinetic constraints is that jamming of particles occurs in directed paths, either paths extending from the South neighbors to the North neighbors, or paths extending from the East neighbors to the West neighbors. Assuming rigid boundary conditions if we restricted only one direction (for example, saying a site is unblocked if its N or S groups are empty, disregarding W and E) then jamming would occur when particles would form a line spanning the system from the top to the bottom wall(see Fig. 1.9a). And if we restrict only the other direction (for instance, require that W or E to be empty for a site to be unblocked) then jamming would occur when particles form a line spanning the system from the left to the right wall. If the line formed does not reach both ends of the system then the particles at the open edge of the line would not be blocked and thus the line of particles will not be frozen. However,when we consider the full rules of the spiral model lines no longer have to reach the edge of the system but instead must only reach other lines and form a T like shape (these are referred to as **T junctions**) which in turn reach to the edges of the system, or to other lines reaching the edge of the system. See Fig. 1.9b for a visual example.

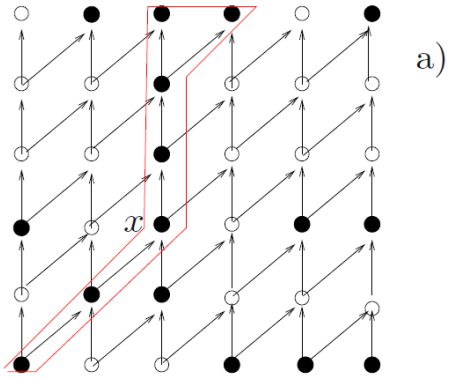

(a) Illustrating the directed paths extending from South to North.

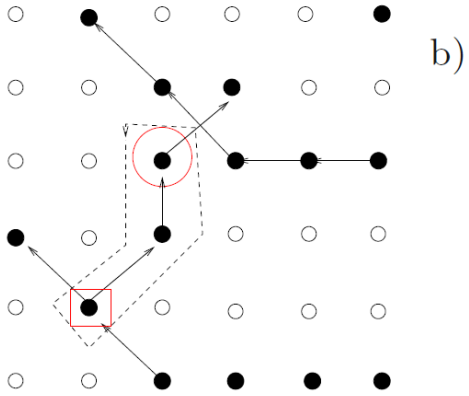

(b) A frozen cluster in the South-North direction bridging two frozen clusters extending in the East-West direction. In order for the particles highlighted by the dashed line to be able to become unblocked particles from one of the East-West clusters must first move. Two types of T junctions are illustrated, one (marked with a square) where the junction site is part of both directed paths, and the other (marked with a circle) where the junction site crosses another directed path but is not contained within the crossing path.

Figure 1.9: Illustration of the frozen directed paths in the spiral model. Adapted from [4].

As noted, the spiral model exhibits a jamming transition of a mixed order nature. The order parameter - the fraction of frozen particles in the system - jumps discontinuously as in a first order transition. However, there also exists a diverging length scale, namely the length of the line of particles that must move before a particle becomes unblocked, which is typical of a second order phase transition [3]. Such a mixed order phase transition is known to occur in the context of glasses and jamming [23, 24, 32].

1.3.5 Sites - Frozen vs Unfrozen

Sometimes instead of looking at particles it is more convenient to look at sites directly [27]. Sites that are permanently blocked are called **frozen sites**, and never change their state. Frozen and **unfrozen sites** could potentially be occupied or vacant. Occupied **frozen sites** would correspond to **frozen particles** while **unfrozen particles** may reside only in **unfrozen sites**. Since frozen sites never change their state, they act as effective walls in the system, since regardless of whether they are occupied or vacant, particles can never jump into them. Similarly, unfrozen sites are sites that can, at some point, change their state, and so these act as free volume where particles can move. Similarly to the jammed particles case, whether a site is frozen or unfrozen is determined when initial conditions are set, and so the connectivity of frozen sites actually determines the underlying structure of the system, determining where and how particles can move.

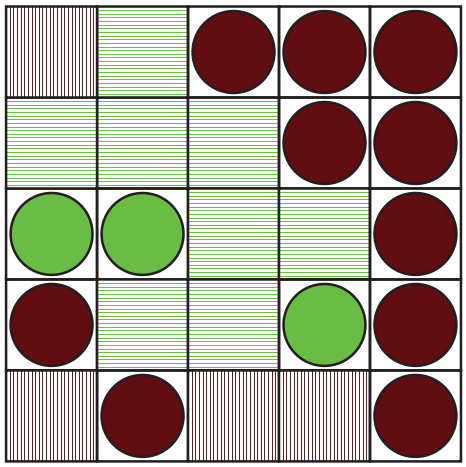

Figure 1.10: Frozen particles and sites in the spiral model (assuming periodic boundary conditions): **Dark red circles**: frozen particles, **bright green circles**: unfrozen particles. **Red vertical shading**: frozen sites, **green horizontal shading**: unfrozen sites. Adapted from [27].

Chapter 2

Objective

2.1 The Model

We have investigated a three dimensional extension to the spiral model first introduced in [11]. Here neighbors of every site on the three-dimensional cubic lattice are divided into six sets, where Top and Bottom were added in addition to North South West and East sets of the spiral model. Here we define six logical variables $\tilde{N}$, $\tilde{S}$, $\tilde{W}$, $\tilde{E}$, $\tilde{T}$ and $\tilde{B}$ which are true if all three sites of their corresponding set are occupied and are false otherwise. For a site to be unblocked the condition $\left(\left(\tilde{N} \vee \tilde{S}\right) \wedge \left(\tilde{W} \vee \tilde{E}\right)\right) \wedge \left(\tilde{T} \vee \tilde{B}\right)$ must be be true, see Fig. 2.1.

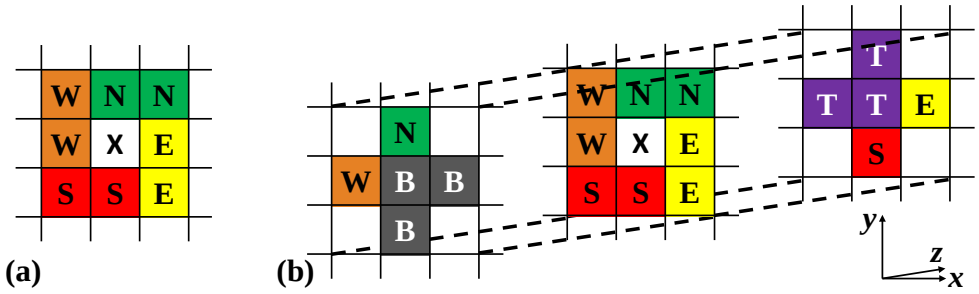

Figure 2.1: **(a)** 2D Spiral model rules. **(b)** 3D Model rules. The central site $[x]$ is unblocked if (N or S) and (W or E) and (T or B) groups are completely empty.

Similarly to the two dimensional case, here there are three perpendicular directed paths (South-North, East-West, and Bottom-Top) and particles may form frozen clusters in any of these path. Due to these more restricting set of rules we may expect $\rho_J^{3D} > \rho_J^{2D}$ and indeed as seen in the top panel of Fig.2.2, $\rho_J^{3D} \approx 0.35$.

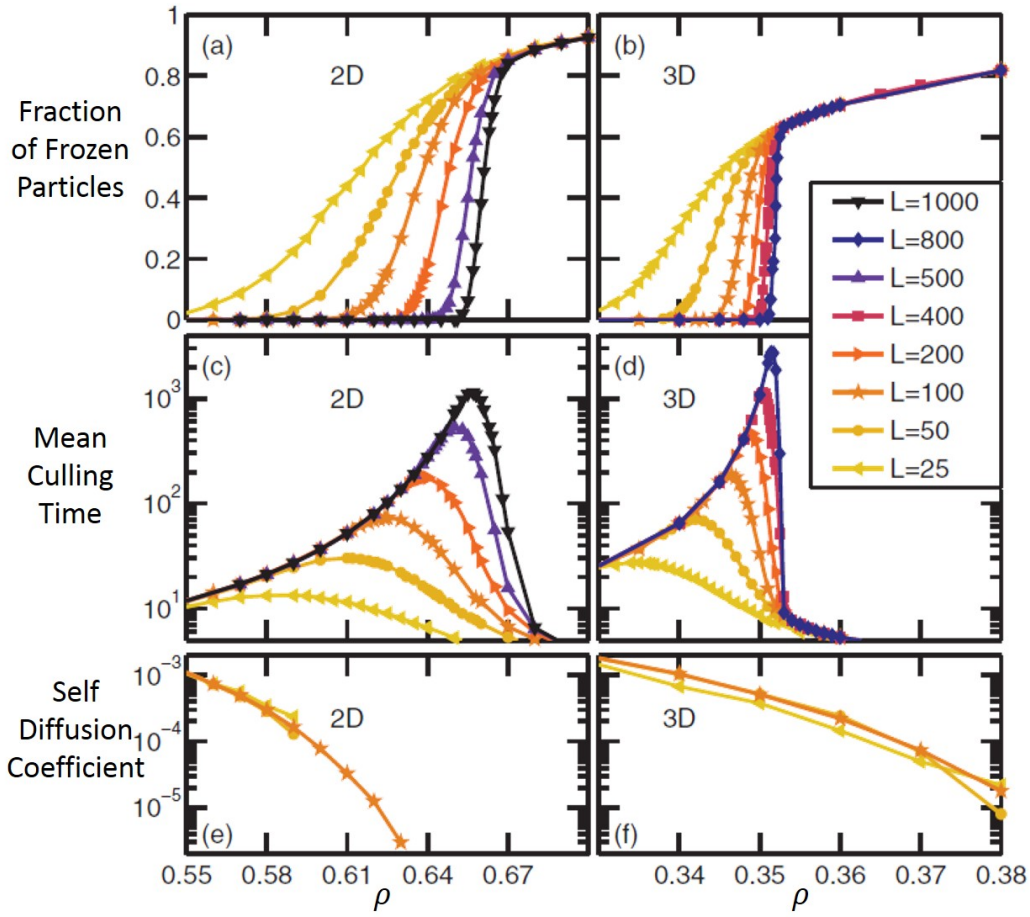

Figure 2.2: Results comparing between the 2D spiral model and the 3D model. **(a,b)** 2D,3D fraction of frozen particles in the system, **(c,d)** 2D,3D Mean culling time - the average number of culling steps required to cull a particle. Culling is explained in chapter 3. **(e,f)** 2D,3D Self diffusion coefficient of the non-frozen particles in the system. Adapted from [11].

2.1.1 Caging

In two dimensions the self diffusion coefficient of mobile particles in the system vanishes at $\rho = \rho_J^{2D}$, however in the three dimensional case as density is increased also beyond ρ_J the self diffusion coefficient does not vanish and thus mobile particles still diffuse freely across the system. The authors of the original paper gave a geometric intuitive explanation, stating that since jamming in these models occurs by the formation of one dimensional clusters, these clusters in two dimensions act as walls caging particles and preventing long range diffusion, but in three dimensions only act as strings that may be bypassed using the third dimension [11]. They then proceed to predict the existence of a second phase transition - a **caging transition** - in the 3D model at ρ_C. This transition occurs when density is increased to the point where these one dimensional frozen clusters become surfaces, thus particles can no longer bypass the frozen clusters of particles and are confined within cavities that are formed within gaps of frozen structures, causing the self diffusion coefficient to vanish.

2.2 Goal

The goal of this work is to show the existence of the previously predicted **caging transition** at ρ_C, and to identify and characterize it. In contrary to past work which relied on running a dynamical simulation of the system over long periods of time, this work aims to answer this question from a structural point of view [34, 21], thus decreasing the computational resources required to achieve this goal. More importantly, the dynamical simulation approach is lacking in the sense that when one measures self diffusion there isn't a known halting condition regarding when to stop measuring the mean square displacement. This makes measuring the caging transition impossible, as you can never be certain if a particle is truly caged. This work presents a more robust approach which uses a deterministic algorithm with a well defined stopping condition which is able to properly measure the caging status of the system.

Chapter 3

Method and Results

3.1 Methods

To determine whether or not the system is in a caging regime we observe clusters formed from the unfrozen sites in the system. The unfrozen sites act as free volume in which particles can potentially move, while the frozen sites - sites that particles cannot move to or from - act as effective walls. Consider a cluster of unfrozen sites with a mass $m \sim L^a$: If a cluster scales as the **volume** of the system, that is $a = d$, then in the thermodynamic limit it is infinite and thus a tracer particle placed in such a cluster would be able to diffuse over long distances. This is certainly an uncaged regime. If a cluster scales with less than the **length** of the system, that is $a < 1$, then it cannot span the system and in the thermodynamic limit it is finite in any dimension (See Fig. 3.1 for a 2D example). A tracer particle in that cluster can only travel in its local environment, and so this is certainly a caged regime.

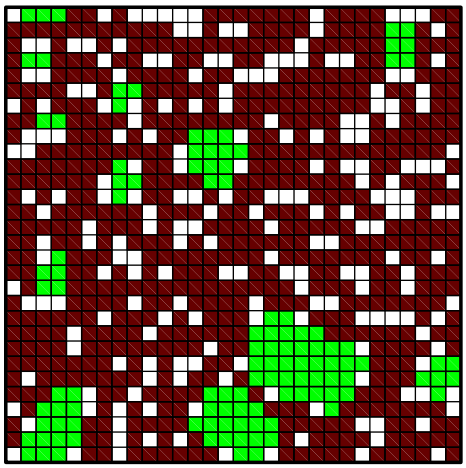

Figure 3.1: A representative configuration of the 2D spiral model at $\rho = 0.69$ for a square lattice of linear size $L = 30$. Frozen particles are marked in dark red, unfrozen sites in bright green. Clusters of unfrozen sites are all finite with their mass scaling as $\sqrt{L}$, and so caging occurs. Adapted from [27].

To find which sites are frozen and which are unfrozen we use culling; a deterministic algorithm which allows the identification of frozen particles [34]. To perform culling on some initial configuration of particles we:

1. Scan the system and find all unblocked particles.
2. Remove all unblocked particles.
3. If no particles were removed, end. Else return to **(1)**.

Put simply, every iteration we identify unblocked particles and delete them. By doing so we may cause neighboring particles to become unblocked. We repeat this until there aren't any more unblocked particles in the system, which may happen in one of two scenarios: Either all particles were removed from the system, and so there aren't any more particles to remove, or the remaining particles in the system are frozen particles and so they will never become unblocked, and so we are left only with particles that are frozen. If so, culling is a useful tool which allows us to identify frozen particles in the system. However, there are some

rare configurations in which culling would delete frozen particles, see Fig. 3.2. These configurations however, can occur only when particles are caged, and even then, in large enough systems should only occur with very few particles and so culling should give a very good lower bound on the number of frozen particles in the system. Since local dynamics of a site depend on the state of its neighbors we can find all frozen **sites** by finding the frozen **particles**, and so after culling had been performed we can easily identify the frozen and unfrozen **sites** in the system.

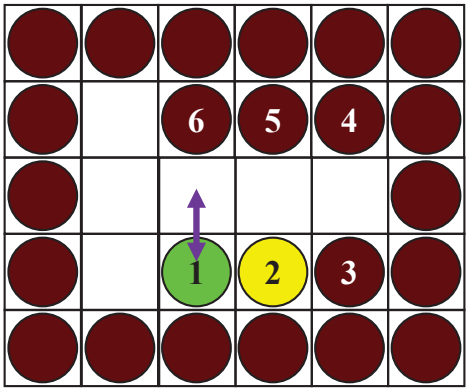

Figure 3.2: Culling versus dynamics: configuration for which culling fails to exactly identify frozen particles in the two dimensional spiral model. In this small region surrounded by occupied sites (red circles) the only possible dynamics are particle 1 moving one site up and then back down, thus it is the only unfrozen particle. However, after particle 1 is culled from the system, particle 2 is culled as well, despite that fact it could not move. Particles 3,4,5 and 6 are properly identified by the culling algorithm as frozen. Adapted from [27].

From this sort of analysis we learn that it may be possible for us to determine the state of the system (caging or not) merely by looking at how these clusters scale with the size of the system, and so we proceed to identify and measure the distribution of the sizes of these clusters. To perform this process we use numerical simulations. We start out by setting a system of size L^d and an initial particle density ρ. We then choose random initial particle positions by going through every site in the system and setting it to be occupied with probability

ρ . After the initial configuration has been decided we use the culling algorithm and are left with a system containing only sites with frozen particles. We then complete this stage by checking every initially vacant site and see if it is frozen or unfrozen. In the last stage we choose an unfrozen site and check which of its neighbors are unfrozen as well, and list those into a cluster together. We iteratively repeat this for the neighbors of the chosen site and their neighbors and so on until no new sites are added to the cluster, in which case we move to another unfrozen site that has not been listed into a cluster yet. When we have listed every unfrozen site in the system into a cluster the process ends. This whole process is repeated over many realizations and for different system sizes and densities. In comparison to previous work [11] this method is significantly less intensive in terms of computational resources as the time complexity is $O\left(L^3\right)$. While the previous paper had reached a system of linear size $L = 100$ when measuring diffusion, here we easily reach systems of linear size $L = 500$, which are 125 times larger in terms of number of sites. More so, given the current memory capacity we have on our computational cluster, and given reasonable running times, we expect to be able to reach as high as systems of linear size $L = 1300$.

3.2 Results

We measured the mass (volume) distribution of clusters of unfrozen sites both in two dimensions and three dimensions. Since we want to study clusters composed of unfrozen sites it will make more sense if we stop using ρ, which only gives us information regarding the particle density in the system, and instead use p, the fraction of unfrozen sites in the system, which gives us information regarding the unfrozen site density directly (see Fig. 3.3). This p is conceptually similar to the p we've seen in percolation problems in Chapter 1. However, unlike the random percolation case, here there are correlations between the locations of unfrozen sites.

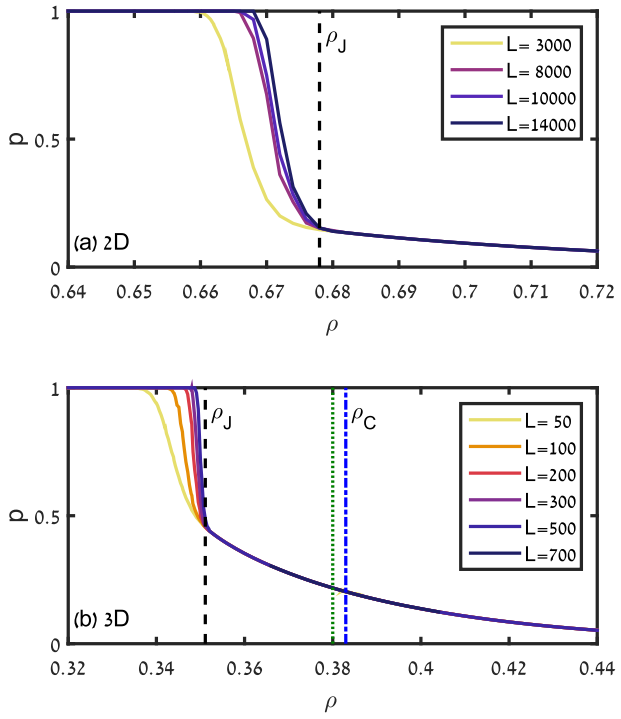

Figure 3.3: **Accessible sites:** fraction p of unjammed, or accessible sites decreases with increasing particle density ρ. For $\rho < \rho_J$ the system is unjammed and $p = 1$. At ρ_J (vertical dashed black line), p jumps discontinuously to a finite value p_J, and then decreases smoothly with increasing ρ. In 2D (panel **(a)**), the system becomes caged at ρ_J, while in 3D (panel **(b)**), the caging transition (vertical blue dash-dotted line) occurs at some higher density ρ_C and does not exhibit there any singularity in $p(\rho)$. In **(b)** the dotted green vertical line represents the highest densities achieved in the 2014 EPL paper[11] by means of dynamical simulations. (achieved for systems up to size $L = 100$). Adapted from [27].

We then use tools from percolation theory to analyze the distribution of clusters, starting with P - the probability a site belongs to the infinite cluster[1]. See Fig. 3.4.

[1]it should be noted that if an infinite cluster does exist, then it is the only infinite cluster in the system[33]

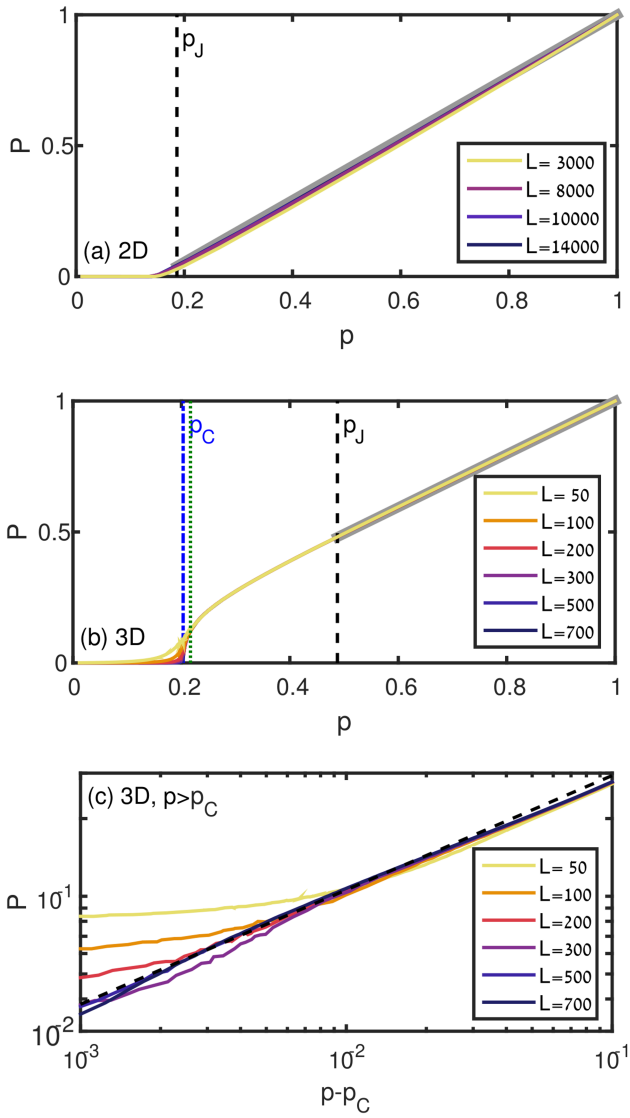

Figure 3.4: **Infinite cluster: (a)**, **(b)** probability that a site belongs to the largest cluster exhibits a continuous percolation transition at p_C (vertical blue dashdotted line) only in the 3D model. In both 2D and 3D, the behavior for $p > p_J$ is characteristic of a discontinuous transition. Namely, only precisely at p_J some of the realizations do not have any frozen particles and some have a finite fraction of frozen particles, thus the measurement averaged over multiple realizations gives a linear interpolation indicated by the thick gray lines. **(c)** In 3D, for $p \gtrsim p_C$, P scales as $P(p - p_C)^\beta$ with $\beta = 0.4$ (black dashed line). In **(b)** the dotted green vertical line represents the highest densities achieved in the 2014 EPL paper[11] by means of dynamical simulations. (achieved for systems up to size $L = 100$). Adapted from [27].

In the two dimensional system at $p > p_J \approx 0.2$ there is an infinite cluster in the system with mass $M = L^2$ which means that $P(p > p_J) = 1$. However as we decrease p to $p < p_J$ the infinite cluster breaks up and we are left only with smaller clusters which scale as $m \sim L^{\frac{1}{2}}$, see Fig. 3.1. These are finite clusters and so $P = 0$. As discussed before, these clusters do not allow non-local motion of particles and so in two dimensions the jamming transition p_J is also the caging transition of the system. In three dimensions at $p > p_J$ there also an infinite cluster with mass $M = L^3$. As p is decreased and we cross the jamming transition $p_J \approx 0.5$ there still an infinite cluster which scales as the volume of the system $M \sim L^3$. However, now it comprises only some fraction of the system ($\frac{M(p<p_J)}{M(p>p_J)} < 1$), see Fig. 3.6 **(a)**. As we continue decreasing p we find a second transition at $p_C \approx 0.2$ in which the infinite cluster breaks down altogether into smaller clusters that scale as $m \sim L^{\frac{1}{2}}$ and found $P(p < p_C) = 0$, see Fig. 3.6 **(b)**. That is, in three dimensions we found two different transitions – the first transition at p_J where particles in the system become frozen and the system jams, and a separate transition at p_C where the clusters of frozen sites start confining particles inside clusters of unfrozen sites. Exactly identifying p_C using this method has proven difficult, and so at this point the exact numerical value of p at which the largest cluster in the system turns from infinite to finite is unknown. This is due to the fact that in a numerical simulation we can only consider finite systems.

To try and find p_C more accurately we measured S - the average finite cluster mass. S by definition must include all finite clusters in the system. As we move closer to $p = p_C$ it becomes harder to conclude whether or not the largest cluster in the system should be included when calculating S (since we are uncertain whether or not we are at $p < p_C$ or $p > p_C$). This makes the task of calculating S rather tricky.

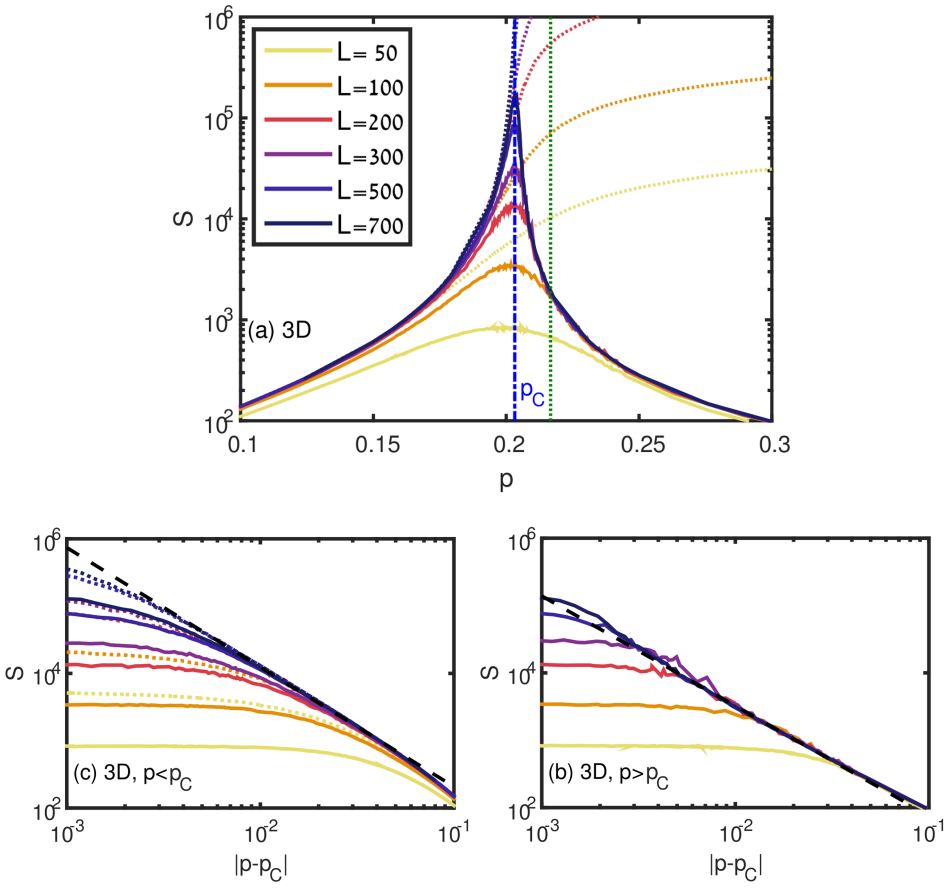

Figure 3.5: **Finite clusters**: **(a)** The average size of a cluster that each site belongs to in the 3D model. Solid lines are S_0 which excludes the largest cluster, and thus peak at the critical density for caging (vertical blue dash-dot line). Dotted lines are S_1 which includes the largest cluster, and thus increase with system size for $p > p_C$ since there a percolating cluster exists. **(b)** For $p > p_C$ we find that $S_0 \propto (p - p_C)^{-\gamma}$ with $\gamma = 1.5$ (black dashed line). **(c)** For $p < p_C$ we find that S_0 (solid lines) and S_1 (dotted lines) behave similarly. However since S_1 reaches larger values we fit it to $S_1 \propto (p_C - p)^{-\gamma}$ with $\gamma = 1.9$ (black dashed line). In **(a)** the dotted green vertical line represents the highest densities achieved in the 2014 EPL paper [11] by means of dynamical simulations. (achieved for systems up to size $L = 100$). Adapted from [27].

To overcome this problem we defined two different S, one denoted by S_0 which takes into account all clusters in the system **excluding** the largest cluster

(even if it is **finite**), and the second by S_1 which takes into account all clusters in the system **including** the largest cluster (even if it is **infinite**). It is worth pointing out that we consider a cluster infinite if it is infinite in the thermodynamic limit. On the right side of the plot at Fig. 3.5 **(a)** at $p > p_C$ the solid line (for S_0) is accurate, as the largest cluster is infinite. On the left side of the plot at $p < p_C$ the dashed line (for S_1) is accurate since the largest cluster is finite. In the center of the plot at $p = p_C$ we observe a maximum in S, diverging with system size.

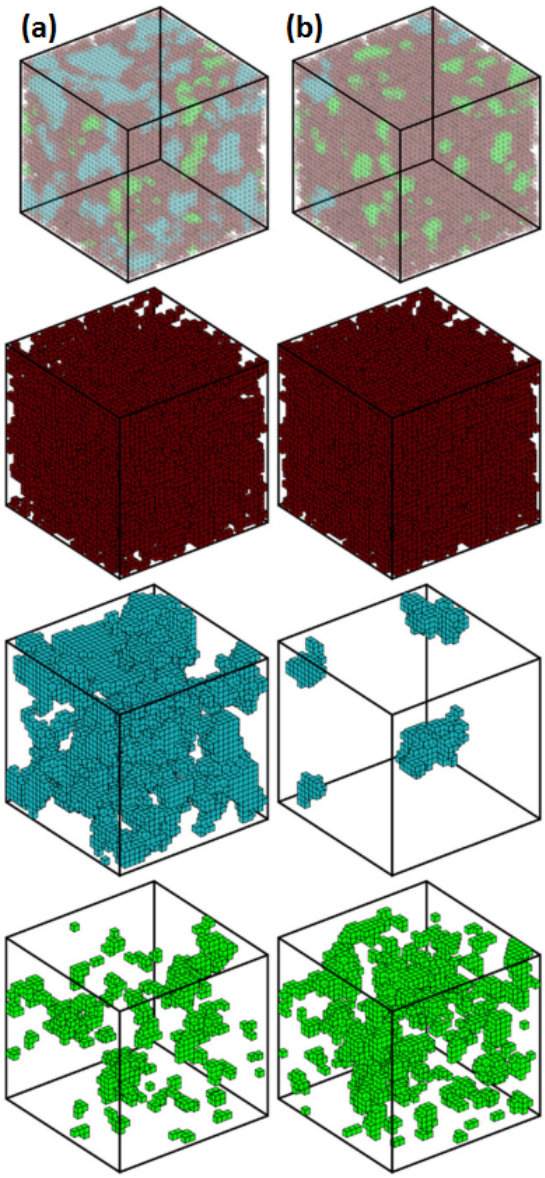

Figure 3.6: Representative configurations of the 3D model at **(a)** $\rho = 0.37$, which is between the jamming density $\rho_J \approx 0.35$ and the caging density $\rho_C \approx 0.38$, and **(b)** $\rho = 0.37$, which is above ρ_C, for a cubic lattice of linear size $L = 30$. Frozen particles are marked in dark red, the largest cluster of unfrozen sites in light blue and unfrozen sites that belong to all other, smaller clusters in bright green. For visualization, we separately copied below each image the three components comprising it. At both densities shown here there are frozen particles, however in **(a)** the largest cluster of unfrozen sites spans the system, while in **(b)** it is compact. Thus the dynamics are predicted to be diffusive for $\rho < \rho_C$ and caged for $\rho > \rho_C$. Adapted from [27].

We numerically calculated the critical exponents for $P \sim (p-p_C)^{\beta}$ and $S \sim (p-p_C)^{-\gamma}$. We found $P \sim (p-p_C)^{0.4}$, $S_0 \sim (p-p_C)^{-1.6}$ and $S_1 \sim (p-p_C)^{-1.8}$ See Fig. 3.4 **(c)** and Fig. 3.5 **(b,c)**.

We also calculated the fractal dimension of the infinite cluster from ($M\,(p=p_C) \sim L^{d_f}$) and the scaling factor for the average cluster size from $S(p_C) \sim L^{\frac{\gamma}{\nu}}$, see Fig. 3.7.

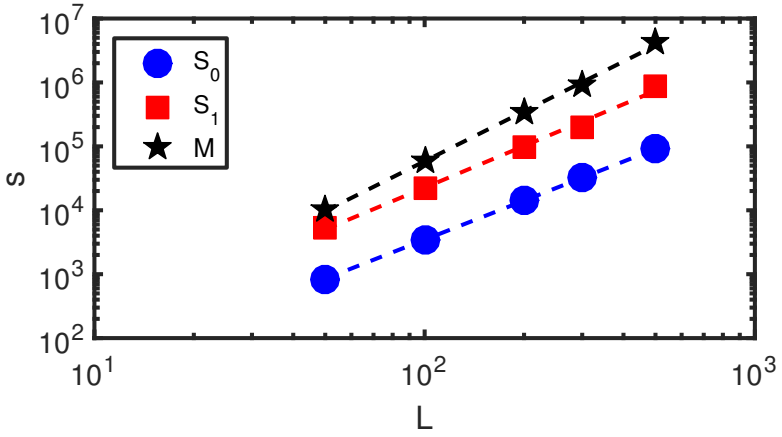

Figure 3.7: The average cluster size at the caging transition scales with the system size as $S_0\,(p_C) \propto S_1\,(p_C) \propto L^2$. The size of the largest cluster scales as $M \propto L^{2.5}$. Adapted from [27].

	3D Model	Random Percolation
d_f	2.5	2.5
β	0.4	0.41
γ	$1.8^{[\star]}$	1.80
$\frac{\gamma}{\nu}$	2	2.05
p_C	0.2	0.31

Table 3.1: Critical exponents, scaling factors and critical densities of the 3D model's caging transition versus those of random percolation. The values we obtained agree with those of RP, varying only in the critical density - and so these two transitions are of the same universality class.
$[\star]$ Taken for $S = S_0$.

These sort of scaling relations as well as the value of the critical exponents and fractal dimension of the infinite cluster as seen in Table. 3.1 are in agreement with those of random percolation[33], however the critical density we find differs from that of random percolation. This can be understood by the difference in initial conditions. In a 3D random percolation problem we randomly choose $p \cdot L^3$ sites and set them to be vacant, and then check their connectivity. However in our 3D model we take random initial conditions and then cull particles in accordance to the model's kinetic constraints, thus resulting in some set of vacant unfrozen sites. This introduces some correlations between the unfrozen sites. However, clusters in this model are rather compact and do not exhibit long range correlations and so one could think of this transition similarly to a random percolation transition of clusters rather than a transition of sites. Of course, these clusters are bigger than a single site and are varying in mass, and so $p_C \neq p_{RP}$ which leads us to conclude that these transitions are of the same universality class but there isn't a one to one mapping between the two.

3.3 Finite Size Scaling

To verify these results and to obtain some measure of the error in the critical exponent, we performed finite size scaling. In a finite system the value of the critical point p_C shifts due to finite size effects. The critical density of a system of finite size L, shifted from p_C is given by [33]:

$$p_{av}(L) = \int_0^1 p \left(\frac{d\Pi}{dp} \right) dp, \tag{3.3.1}$$

where $\Pi(p, L)$ is the probability an infinite cluster exists in a system of size L at density p. At $p = 1$, $\Pi = 1$ and at $p = 0$, $\Pi = 0$, and so we can integrate by parts to simplify the expression:

$$p_{av} = 1 - \int_0^1 \Pi dp. \tag{3.3.2}$$

The square of the width of the transition is given by [33]:

$$\Delta^2 = \int_0^1 (p - p_{av})^2 \left(\frac{d\Pi}{dp}\right) dp. \tag{3.3.3}$$

Integrating by parts lets us obtain

$$\Delta^2 = 2\int_0^1 \Pi dp - \left(\int_0^1 \Pi dp\right)^2 - 2\int_0^1 p\Pi dp. \tag{3.3.4}$$

We know [33]:

$$p_{av}(L) - p_C \propto \Delta(L), \tag{3.3.5}$$

and so we can plot $p_{av}(L)$ as a function of $\Delta(L)$ and extrapolate to $\Delta \to 0$ to find p_C. See Fig 5 in the appendix.

Since these are finite systems we must set a criterion for when ξ_1 the mass of the largest cluster in the system is considered infinite. We say that it is considered infinite if it is greater or equal to some arbitrary value ϕ, which we must choose. At $p < p_C$, $\xi_1 \propto L^{0.5}$. At $p > p_C$, $\xi_1 = L^3$. And so we may choose any ϕ to scale with L in any functional form between these two expressions, and the result will not change in the thermodynamic limit [33]. The choice of ϕ merely affects how quickly we converge to the result. Choosing ϕ will set a criterion for each realization, determining whether Π is zero or one:

$$\Pi(p, L) = \begin{cases} 1 & \xi_1(p, L) \geq \phi \\ 0 & \xi_1(p, L) < \phi \end{cases}. \tag{3.3.6}$$

At the critical point $\xi_1(p_C) = A \cdot L^{2.5}$, A simply being the prefactor obtained from a numerical fit. We tested many possible values of ϕ, and found that for our data $\phi = \frac{A}{4} \cdot L^{2.5}$ gives the best results.

Given some parameter K that scales as $|p - p_c|^{-\kappa}$, if we plotted $L^{-\frac{\kappa}{\nu}}K$ as a function of $L^{-\frac{1}{\nu}}|p - p_c|$ for different values of L, near the critical point the different lines would collapse on the same curve [33]. Therefore, if the values we

found for β, γ and ν are correct we should see a collapse. See Fig. 3.8.

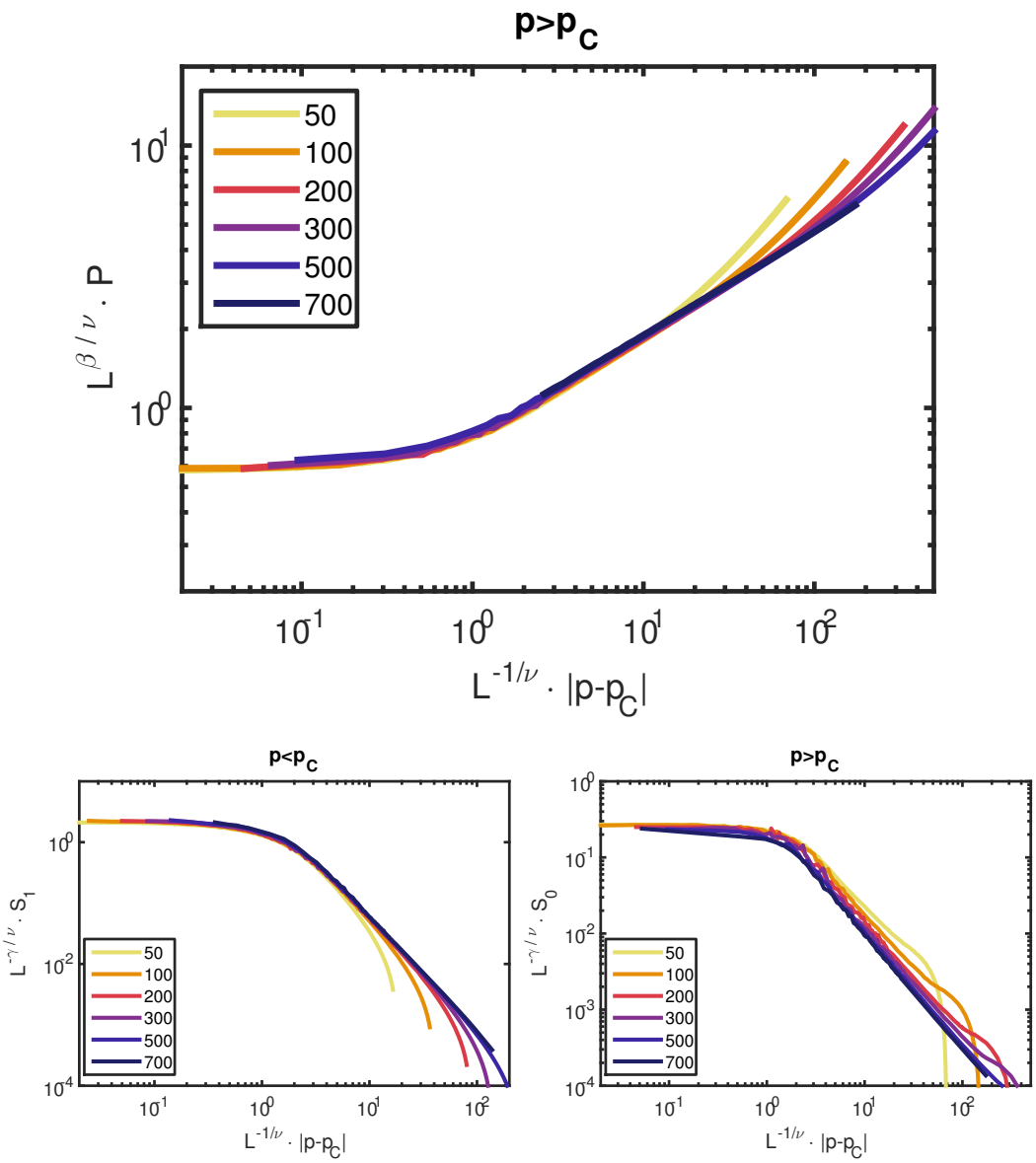

Figure 3.8: **Finite size scaling: (a) - Infinite cluster, (b) Mean cluster, $p < p_C$, (c) Mean cluster $p > p_C$.** Near the critical point all curves collapse one on the other indicating correct values for critical exponents.

It seems we can change the values of the critical exponents by up to 10% and still get a reasonable data collapse, but not more than that, indicating that the relative error in the critical exponents is approximately $\sim 10\%$. See Fig. 1, 2, 3, 4 in the appendix.

Chapter 4

Conclusions

Using numerical simulations considering only the static structure of the system we have shown the existence of the previously predicted caging transition in the 3D model and found the critical unfrozen site density for caging $p_C \approx 0.2$. This static structure method - using the culling algorithm - is significantly faster and cheaper in terms of computational time and computational memory than the straight forward alternative of running the system's dynamics and tracking particle mean square displacement [11]. We have shown how in this critical density p_C the infinite cluster of unfrozen sites breaks down into numerous finite clusters which do not facilitate long range particle diffusion. While the jamming transition in this model is related to a directed percolation transition, we have shown that this new caging transition is actually a random percolation transition, where finite clusters of unfrozen sites band together to form the infinite clusters at $p > p_C$ - this is unlike the two dimensional system where there is only a single transition and caging and jamming occurs at the same critical density.

It is interesting to note the relation to another recently-studied correlated percolation problem, referred to as no-enclaves percolation [30], in which the structure of clusters requires a geometric support, which has some resemblance to the orientational condition of the kinetic constraint that we study. In no-enclave percolation clusters that are contained within other clusters become merged,

thus creating a single large cluster. It would be beneficial to analytically study the caging transition that we have identified and additionally to explore these phenomena in higher dimensions, as it is often the case that models can be analytically solved in higher dimensions, and there is much that can be learned from generalizing the dimension of the model. Moreover, it would be interesting to identify additional models and systems in which jamming is decoupled from caging. A possible direction could be relating our findings to other glassy models exhibiting multiple distinct transitions [28, 29].

The original paper describing the 3D model [11] had a proof of the existence (and critical density value) of the jamming transition. However, this proof was found to be false, only showing that the critical density $\rho_J \leq \rho_{DP}^{3D}$. The current continuation of this work is an attempt to numerically find the critical density ρ_J of the transition and show it behaves according to the directed percolation universality class by using tools similar to those used in this current work. We intend to follow the same method used in [37], which applied this sort of proof for the Knights Model [36] in two dimensions.

Bibliography

[1] H C. Andersen and W. Kob. Testing mode-coupling theory for. *Physical Review E*, 52(4), 1995.

[2] C. A. Angell. Formation of Glasses from Liquids and Biopolymers. *Science*, 267(5206):1924, 1995.

[3] L. Berthier and G. Biroli. Theoretical perspective on the glass transition and amorphous materials. *Reviews of Modern Physics*, 83(2):587, 2011.

[4] G. Biroli and C. Toninelli. Spiral model, jamming percolation and glass-jamming transitions. *European Physical Journal B*, 64(3-4):567, 2008.

[5] J. Chalupa, P. L. Leath, and G. R. Reich. Bootstrap percolation on a Bethe lattice. *Journal of Physics C*, 12:L31, 1978.

[6] K. Christensen, H. Flyvbjerg, and Z. Olami. Self-Organized Critical Forest-Fire Model: Mean-Field Theory and Simulation Results in 1 to 6 Dimensions. *Physical Review Letters*, 71(17):2737, 1993.

[7] A. Coniglio, H. E. Stanley, and W. Klein. Site-bond correlated-percolation problem: A statistical mechanical model of polymer gelation. *Physical Review Letters*, 42(8):518, 1979.

[8] A. S. De Wijn, D. M. Miedema, B. Nienhuis, and P. Schall. Criticality in dynamic arrest: Correspondence between glasses and traffic. *Physical Review Letters*, 109(22):1, 2012.

[9] P. Debenedetti and F. H. Stillinger. Supercooled liquids and the glass transition. *Nature*, 410(6825):259, 2001.

[10] G. H. Fredrickson and H. C. Andersen. Kinetic Ising Model of the Glass Transition. *Physical Review Letters*, 53(13):1244, 1984.

[11] A. Ghosh, E. Teomy, and Y. Shokef. Jamming percolation in three dimensions. *EPL (Europhysics Letters)*, 106(1):16003, 2014.

[12] H. Hinrichsen. Non-equilibrium critical phenomena and phase transitions into absorbing states. *Advances in Physics*, 49(7):815, 2000.

[13] A. E. Holroyd. Sharp metastability threshold for two-dimensional bootstrap percolation. *Probability Theory and Related Fields*, 125(2):195, 2003.

[14] J. Jäckle. Models of the Glass Transition. *Reports on Progress in Physics*, 49:171, 1986.

[15] M. Jeng and Shwarz J. M. Force-balance percolation. *Physical Review E*, 81(011134):1, 2010.

[16] M. J. Keeling. The effects of local spatial structure on epidemiological invasions. *Proceedings of the Royal Society of London B*, 266(1421):859, 1999.

[17] W. Kob. a test of mode-coupling theory of the ideal-glass transition. *Physical Review Letters*, 48(6):4364, 1993.

[18] D. Landau and K. Binder. *A Guideto Monte Carlo Simulations in Statistical Physics*. New York: Cambridge University Press, 2009.

[19] S. Léonard and P. Harrowell. Macroscopic facilitation of glassy relaxation kinetics: Ultrastable glass films with frontlike thermal response. *Journal of Chemical Physics*, 133(24):244502, 2010.

[20] C. T. MacDonald, J. H. Gibbs, and A. C. Pipkin. Kinetics of biopolymerization on nucleic acid templates. *Biopolymers*, 6(1):1, 1968.

[21] M.L Manning and A. J. Liu. Vibrational Modes Identify Soft Spots in a Sheared Disordered Packing. *Physical Review Letters*, 107(10):108302, 2011.

[22] M. E. J Newman. Spread of epidemic disease on networks. *Physical Review E*, 66(1):1, 2002.

[23] C. S. O'Hern, S. A. Langer, A. J. Liu, and S. R. Nagel. Random Packings of Frictionless Particles. *Physical Review Letters*, 88(7):075507, 2002.

[24] C. S. O'Hern, L. E. Silbert, A. J. Liu, and S. R. Nagel. Jamming at zero temperature and zero applied stress: The epitome of disorder. *Physical Review E*, 68(1):011306, 2003.

[25] F. Ritort and P. Sollich. Glassy dynamics of kinetically constrained models. *Advances in Physics*, 52(4):219, 2003.

[26] J. M. Schwarz, A. J. Liu, and L. Q. Chayes. The onset of jamming as the sudden emergence of an infinite k-core cluster. *EPL (Europhysics Letters)*, 73(4):560, 2006.

[27] N. Segall, E. Teomy, and Y. Shokef. Jamming vs. Caging in Three Dimensional Jamming Percolation. *Journal of Statistical Mechanics: Theory and Experiment*, page 054051, 2016.

[28] M. Sellito. Cooperative heterogeneous facilitation: Multiple glassy states and glass-glass transition. *Physical Review E*, 86(3):030502, 2012.

[29] M. Sellito. Disconnected glass-glass transitions and swallowtail bifurcations in microscopic spin models with facilitated dynamics. *Journal of Chemical Physics*, 138(22):224507, 2013.

[30] M. Sheinman, A. Sharma, J. Alvarado, G. H. Koenderink, and F. C. MacKintosh. Anomalous Discontinuity at the Percolation Critical Point of Active Gels. *Physical Review Letters*, 114(9):098104, 2015.

[31] G. Shreyas, A.K. Sood, and G. Rajesh. Deconstructing the glass transition through critical experiments on colloids. *Advances in Physics*, 65(4):363, 2016.

[32] L. E. Silbert, A. J. Liu, and S. R. Nagel. Vibrations and Diverging Length Scales Near the Unjamming Transition. *Physical Review Letters*, 95(9):098301, 2005.

[33] D. Stauffer and A. Aharony. *Introduction to Percolation Theory*. Number 4. London: Taylor & Francis, 1991.

[34] E. Teomy and Y. Shokef. Relation between structure of blocked clusters and relaxation dynamics in kinetically constrained models. *Physical Review E*, 92(3):032133, 2015.

[35] C. Toninelli, G. Biroli, and D. S. Fisher. Spatial structures and dynamics of kinetically constrained models of glasses. *Physical Review Letters*, 92(18):185504, 2004.

[36] C. Toninelli, G. Biroli, and D. S. Fisher. Jamming percolation and glass transitions in lattice models. *Physical Review Letters*, 96(3):035702, 2006.

[37] C. Toninelli, G. Biroli, and D. S. Fisher. Toninelli, Biroli, and Fisher Reply: On the universality of jamming percolation. *Physical Review Letters*, 98(12):129602, 2007.

Appendix: Finite Size Scaling Error Plots

This appendix contains plots of $L^{\frac{\beta}{\gamma}}P$ as a function of $L^{-\frac{1}{\nu}}|p-p_C|$ for $p<p_C$, $L^{-\frac{\gamma}{\gamma}}S_1$ as a function of $L^{-\frac{1}{\nu}}|p-p_C|$ for $p<p_C$ and $L^{-\frac{\gamma}{\gamma}}S_0$ as a function of $L^{-\frac{1}{\nu}}|p-p_C|$ for $p>p_C$. The values of the critical exponents were shifted by $\pm 10\%$ and $\pm 20\%$ as described in each figure's description, as to give some indication to the relative error of the values of the critical exponents calculated. A plot of $p_{av}(L)$ as a function of $\Delta(L)$ is also included. See Section 3.3 for further details.

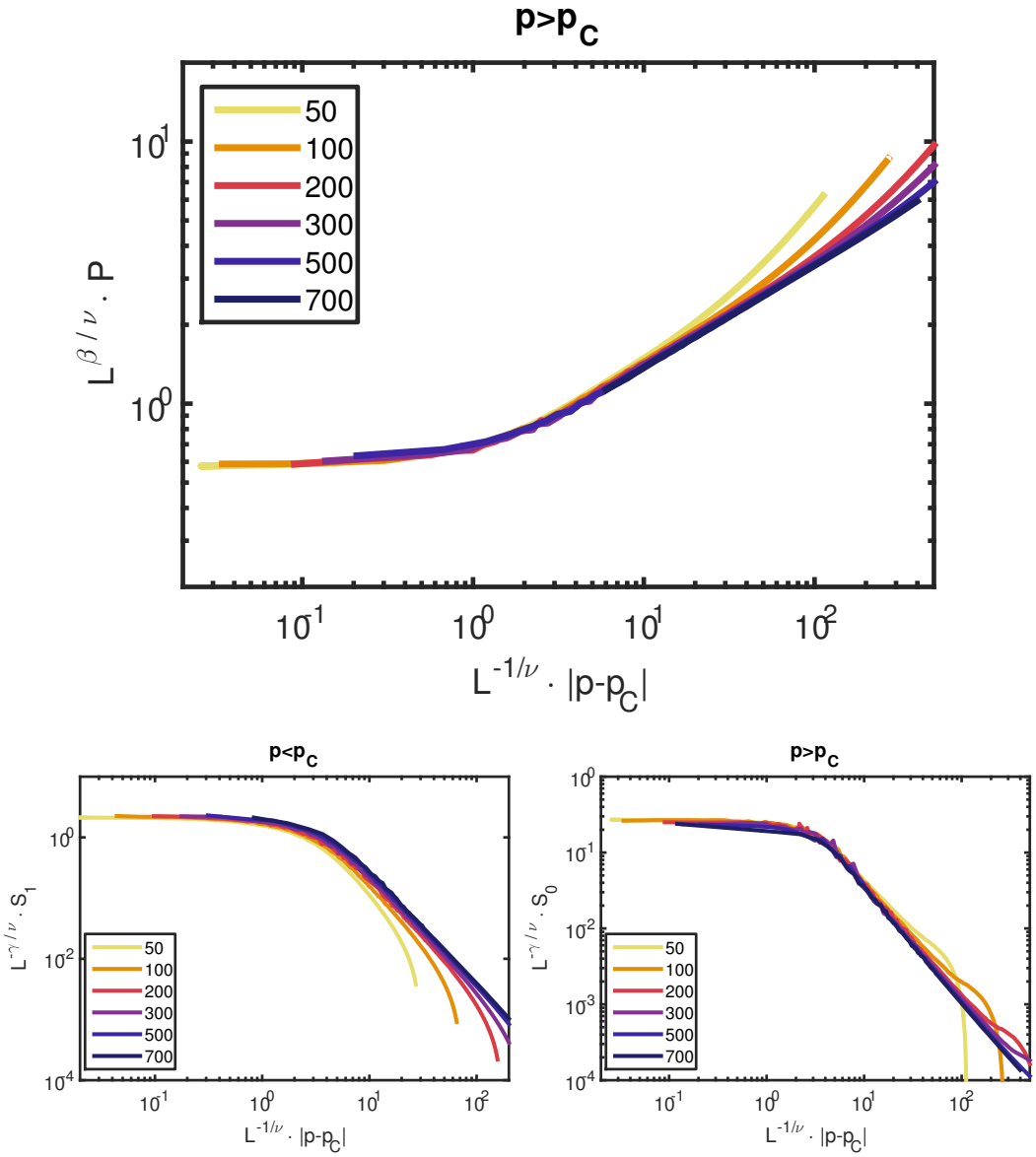

Figure 1: **Finite size scaling: (a) - Infinite cluster, (b) Mean cluster,** $p < p_C$**, (c) Mean cluster** $p > p_C$**.** $\beta \to 0.9\beta$, $\gamma \to 0.9\gamma$, $\nu \to 0.9\nu$.

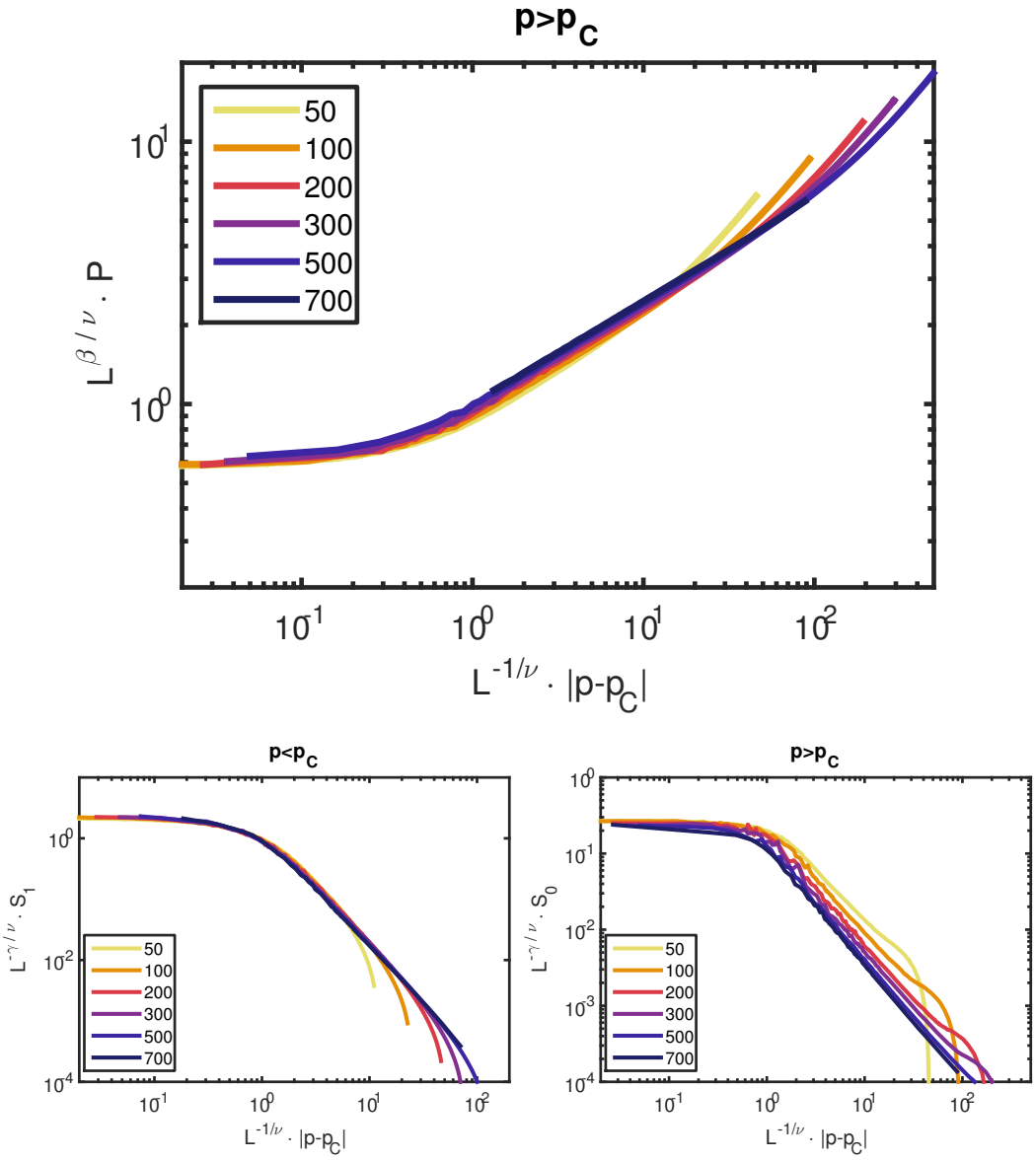

Figure 2: **Finite size scaling: (a) - Infinite cluster, (b) Mean cluster,** $p < p_C$**, (c) Mean cluster** $p > p_C$**.** $\beta \to 1.1\beta$, $\gamma \to 1.1\gamma$, $\nu \to 1.1\nu$.

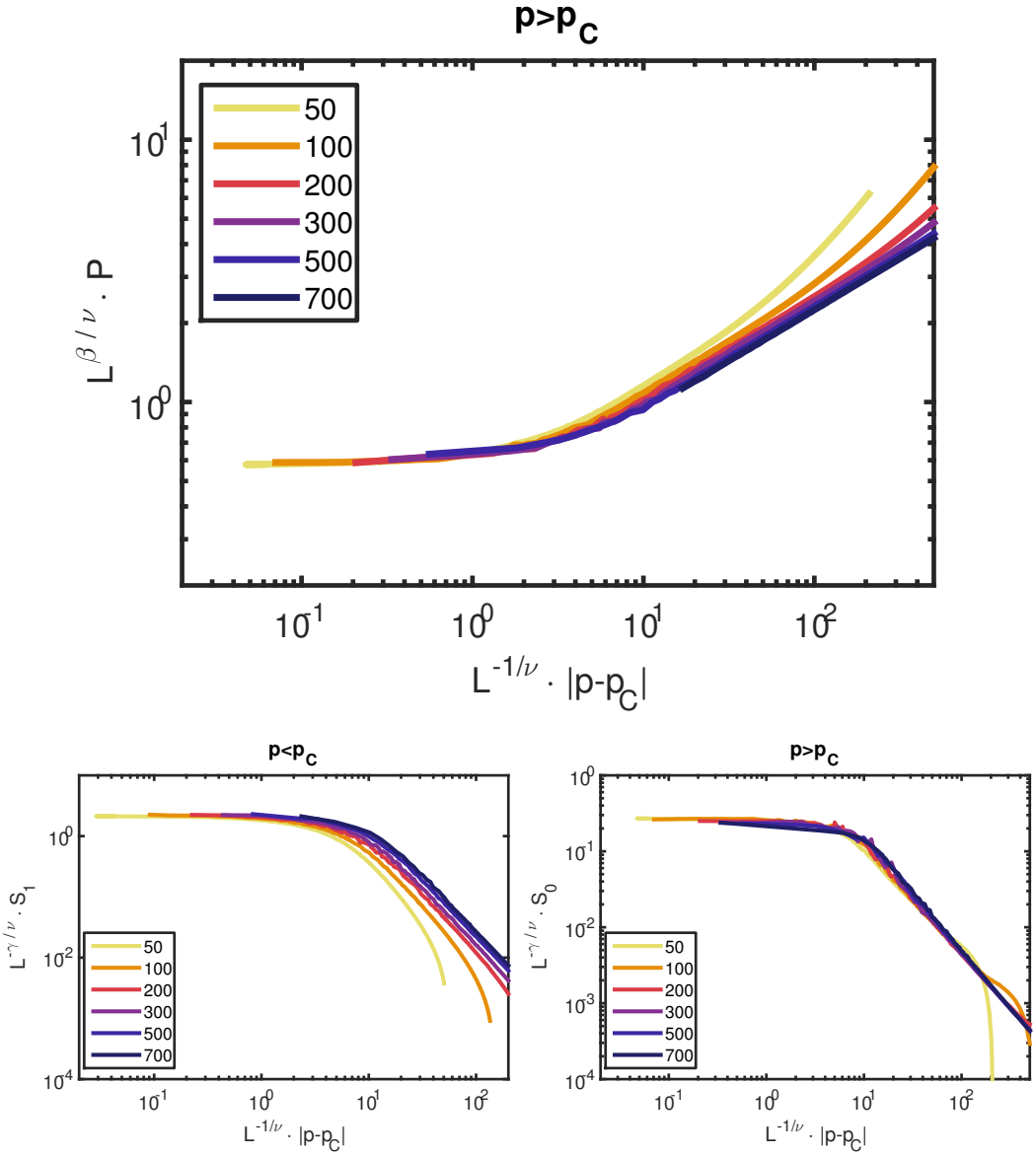

Figure 3: **Finite size scaling: (a) - Infinite cluster, (b) Mean cluster, $p < p_C$, (c) Mean cluster $p > p_C$.** $\beta \to 0.8\beta$, $\gamma \to 0.8\gamma$, $\nu \to 0.8\nu$.

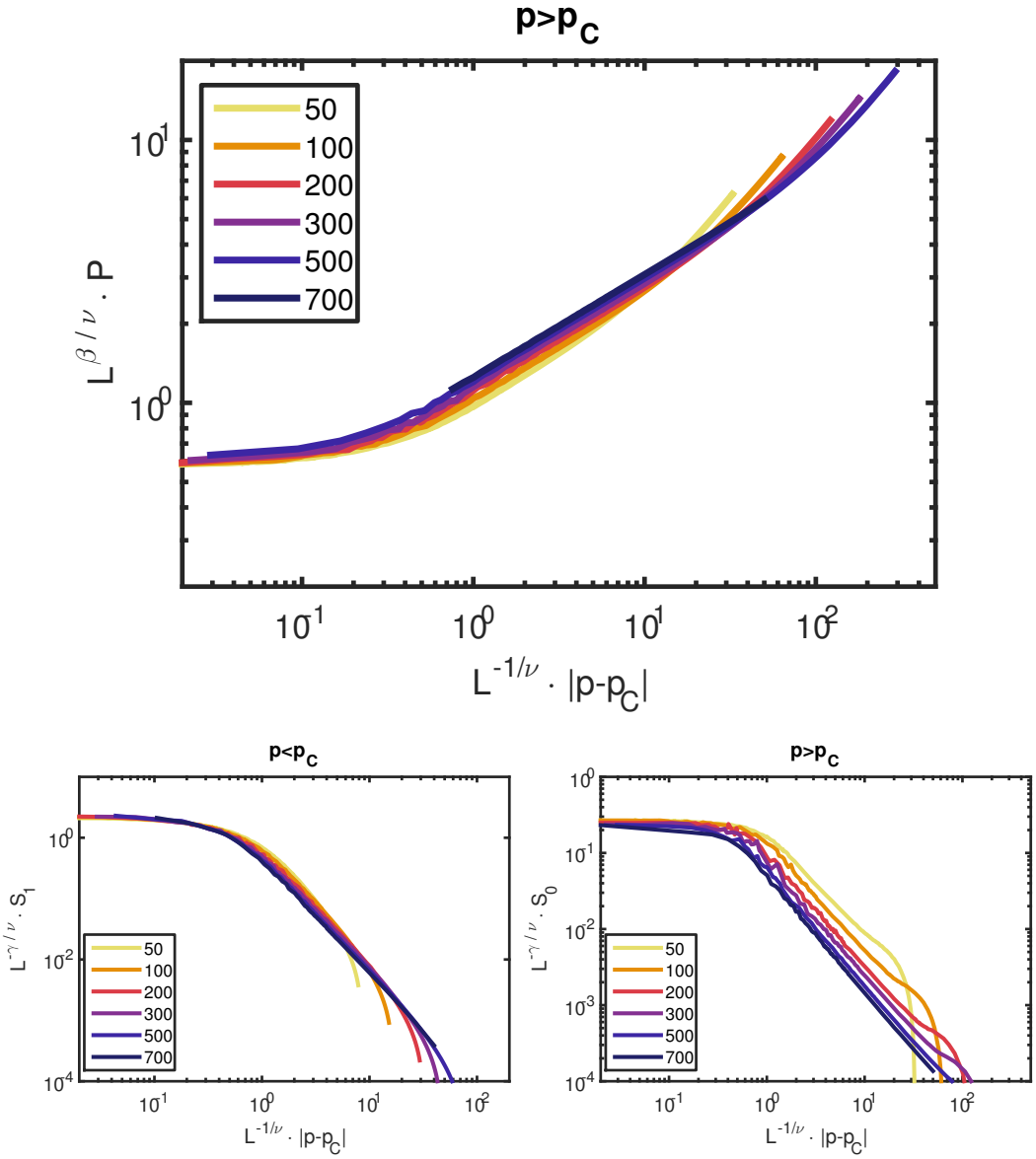

Figure 4: **Finite size scaling: (a) - Infinite cluster, (b) Mean cluster,** $p < p_C$**, (c) Mean cluster** $p > p_C$**.** $\beta \to 1.2\beta$, $\gamma \to 1.2\gamma$, $\nu \to 1.2\nu$.

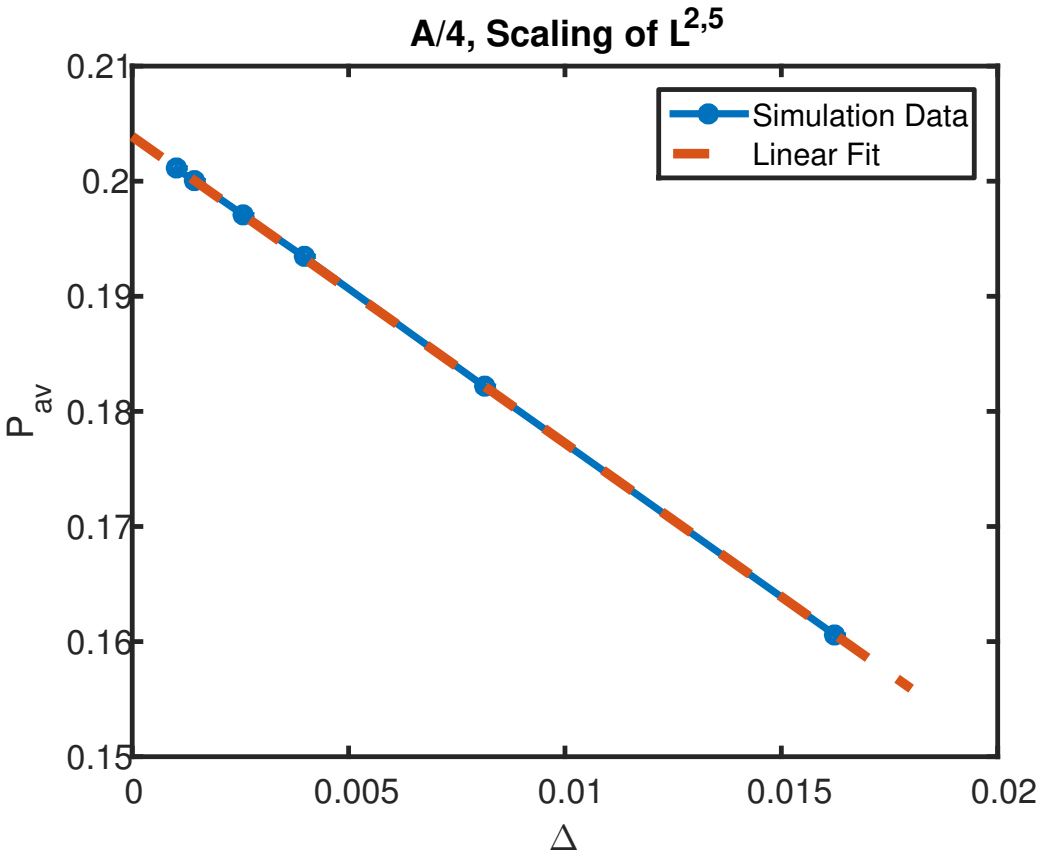

Figure 5: p_{av} *vs.* Δ. At the extrapolated intersect $\Delta = 0$, $p_{av} = p_C$. The linear fit gives $p_{av} = -2.67\Delta + 0.20$ which yields $p_C = 0.20$.

תקציר

זכוכיות מופיעות בחיי היומיום באופן נפוץ, החל מזגוגיות רכב למסך מגע בטלפונים חכמים, למעטפת של נורת להט ועד לכוסות מטבח. בזמן שניתן לשלוט בתכונות הפיזיקליות של זכוכיות המיוצרות באופן תעשייתי בצורה מדויקת, עדיין חסרה הבנה מעמיקה של זכוכיות, ובפרט של מעבר הזכוכית – התהליך שבו חומר הופך לזכוכיתי - ואין תאוריה יחידה המסוגלת להסביר היטב את המהות של התנהגות זכוכיתית. כתוצאה מכך פותחו כלים שונים וגישות שונות רבות במטרה להבין טוב יותר זכוכיות.

אחד מיני הכלים הללו הוא מודלים מאולצים קינטית. מדובר במודלים פשטניים בהם אין אינטראקציה בין חלקיקים והתנועה של חלקיקים מוגבלת בצורה שתלויה באיכלוס של אתרים שכנים. בכימיה ובפיזיקה השימוש העיקרי במודלים האלה קשור בניסיון ללמוד על התקעות - מצב שבו חלקיקים במערכת מגבילים את התנועה של שכניהם כך שחלקיקים מפסיקים לזוז - במערכות שונות. רוב המודלים הללו אינם נתקעים בגבול התרמודינמי, פרט למצב בו כל המערכת מאוכלסת. מנגד, קיימים מספר מודלים כאלה שכן נתקעים גם בצפיפות נמוכה יותר, כמו לדוגמא המודל הספירלי, ומודל הפרשים.

במודל הספירלי הדו ממדי כאשר הצפיפות מגיעה לצפיפות ההיתקעות הקריטית חלק מהחלקיקים במערכת אינם יכולים לזוז יותר והם קופאים. החלקיקים הלא קפואים הנותרים במערכת נכלאים בתוך כלובים שנוצרים מחלקיקים קפואים, ומקדם הדיפוזיה העצמית שלהם מתאפס. במאמר שפורסם באחרונה נידון מודל תלת ממדי המרחיב את המודל הספירלי הדו ממדי. הכותבים הדגימו כי בצפיפות הקריטית להיתקעות החלקיקים הלא קפואים לא נכלאים, ומקדם הדיפוזיה שלהם לא מתאפס. ההבדל נובע מכך שבמערכות הללו חלקיקים נתקעים יוצרים מבנים חד-ממדים אשר מגבילים את התנועה של חלקיקים ניידים. במקרה הדו ממדי המבנים החד ממדיים הללו מהווים קירות שחלקיקים לא יכולים לחצות, בעוד שבמקרה התלת-ממדי חלקיקים עוקפים את המבנים הללו דרך הממד השלישי. הכותבים חוזים את קיומו של מעבר פאזה נוסף בצפיפות גבוהה יותר אשר בו חלקיקים יכלאו בכלובים ומקדם הדיפוזיה שלהם יתאפס.

בעבודה זו אנחנו משתמשים באלגוריתם מהיר ודטרמיניסטי כדי לחשוף את המבנה הבסיסי של המערכת אשר מורכב מאתרים שאינם קפואים – אוסף האתרים במערכת שמהווים נפח חופשי לתנועת חלקיקים, מה שמאפשר לנו להימנע מלהריץ את הדינמיקה של המערכת. אנו משתמשים בתכונה המבנית הזאת של המערכת בכדי לקבוע אם המערכת כולאת חלקיקים לסביבתם הקרובה או מאפשרת דיפוזיה לטווח ארוך ואנחנו מוצאים את הצפיפות הקריטית לכליאה במערכת ומאפיינים את מעבר הפאזה. אנו מוצאים כי בזמן שמעבר הפאזה הראשון במערכת – מעבר הפזה שאחראי להיתקעות – הוא מעבר פרקולציה מכוונת (Directed Percolation), למעבר הפאזה השני הקשור בכליאה יש מעריכי חזקה קריטיים כשל מעבר הפרקולציה האקראית (Random Percoltion), מה שהופך את שני המעברים הללו למעברים מאותה מחלקת שקילות.

אוניברסיטת תל אביב

הפקולטה למדעים מדוייקים

ע"ש ריימונד ובברלי סאקלר

היתקעות לעומת כליאה במודל זכוכיתי תלת ממדי

חיבור זה הוגש כדרישה חלקית לקבלת התואר

מוסמך אוניברסיטה באוניברסיטת תל אביב

בית הספר לכימיה

המחלקה לכימיה פיזיקלית

הוגש על ידי

נמרוד סגל

העבודה בוצעה תחת הדרכתם של

ד"ר יאיר שוקף ופרופ' חיים דיאמנט

כסלו התשע"ז